MASTERARBEIT | MASTER'S THESIS

Titel | Title

Molecular Dynamics Simulation of the Gβ1γ2 Complex Carrying the G64V Mutation Associated with GNB1 Encephalopathy

verfasst von | submitted by

Anna Xhuvani BSc

angestrebter akademischer Grad | in partial fulfilment of the requirements for the degree of

Magistra pharmaciae (Mag. pharm.)

Wien | Vienna, 2026

Studienkennzahl lt. Studienblatt | Degree programme code as it appears on the student record sheet:	UA 066 605
Studienrichtung lt. Studienblatt | Degree programme as it appears on the student record sheet:	Masterstudium Pharmazie
Betreut von | Supervisor:	Assoz. Prof. Mag. Dr. Anna Weinzinger Privatdoz.

Danksagung

Zunächst möchte ich mich bei Frau Assoc. Prof. Mag. Dr. Anna Weinzinger, Privatdoz., herzlich bedanken. Durch ihre Expertise durfte ich Teil ihres Forschungsteams werden und habe in dieser Zeit unglaublich viel lernen können. Ich schätze mich sehr glücklich, dass sie mir die Möglichkeit gegeben hat, meine Masterarbeit unter ihrer fachkundigen Betreuung zu verfassen. Ich möchte Ilia Steshin besonders danken, der immer zur Stelle war, wenn ich Fragen hatte, und mich dabei unterstützte, das Thema besser zu verstehen, die Relevanz der Forschung zu erkennen und verschiedene Blickwinkel auf das Thema einzunehmen.

Mein Dank gilt auch dem gesamten Department für Pharmakologie und Toxikologie für die inspirierende und lehrreiche Zeit, die ich dort erleben durfte.

Von Herzen danke ich meinen Eltern, Arben und Silvana Xhuvani, die in den frühen 1990er Jahren aus Albanien nach Deutschland geflohen sind, in der Hoffnung auf ein besseres Leben für sich und ihre Kinder. Ich werde immer dankbar dafür sein, dass sie ihre eigenen Träume zurückstellten, um uns Kindern Bildung ohne Kompromisse zu ermöglichen und uns stets zu fördern. Ebenso danke ich meinen Schwestern Luise, Francesca und Chiara, die mich immer unterstützt, motiviert und mir stets zur Seite gestanden haben, auch wenn uns manchmal große Entfernungen trennten.

Zusammenfassung

Gβγ-Dimere sind die grundlegenden Bestandteile der GPCR-Signalkaskade (G-Protein-gekoppelte Rezeptoren), die aus sich ausfolgenden Untereinheiten zusammensetzen: Alpha-, Beta- und Gamma. Diese Dimere sind die Hauptbestandteile der Signalkaskade von GPCRs sowohl an intrazelluläre als auch an membrangebundene Effektoren. Die Aufgabe des GNB1-Gens besteht in der Kodierung der Beta-1-Untereinheit des G-Proteins, welche essenziell für die Stabilität des Gαβγ1-Komplexes ist. Punktmutationen im GNB1-Gen führen zur sogenannten GNB1-Enzephalopathie (kurz GNB1-E), einer seltenen genetischen Erkrankung, die folgende Symptome auslösen kann:

- Verlust motorischer Fähigkeiten
- Kognitive Beeinträchtigungen
- Epileptische Anfälle
- Sensorische Defizite

In dieser Arbeit wurde die Punktmutation G64V untersucht, welche die Funktionalität des Gβ1γ-Dimers beeinträchtigt und damit die G-Protein-Signalwege stört. Um die Auswirkungen und Konsequenzen dieser Punktmutation im Detail zu untersuchen, wurden computergestützte molekulardynamische (MD) Simulationen genutzt.

Abstract

Gβγ dimers are fundamental components of the GPCR signaling cascade (G-protein-coupled receptors), which consists of alpha, beta, and gamma subunits. These dimers transmit signals from GPCRs to both intracellular and membrane bound effectors. The GNB1 gene encodes the beta 1 subunit of the G protein. Mutations in the GNB1 gene lead to GNB1 encephalopathy, abbreviated as GNB1-E, which is a rare genetic disorder characterized by

- Loss of motor skills
- Cognitive impairments
- Epileptic seizures
- Sensory deficits

A specific pathogenic point mutation, G64V, severely impairs the functionality of the Gβ1γ dimer, thereby disrupting G protein signaling pathways. To investigate the impact and consequences of this point mutation in detail, computational molecular dynamics (MD) simulations were performed.

Table of content

List of abbreviations

ADHD	Attention Deficit Hyperactivity Disorder
BiFC	Bimolecular Fluorescence Complementation
BRET	Bioluminescence Resonance Energy Transfer
CSF	Cerebrospinal Fluid
Cryo- EM	Cryogenic Electron Microscopy
D1R	Dopamine D1 Receptor
GDP	Guanosine Diphosphate
GDD	Global Developmental Delay
GFP	Green Fluorescent Protein
GIRK	G - Protein–Gated Inwardly Rectifying Potassium Channel
GNB1	Guanine Nucleotide -Binding Protein Beta Subunit 1
GNB1- E	GNB1 Encephalopathy
Gβ1	G beta 1 subunit
Gγ7	G gamma 7 subunit
Gαolf	G alpha olfactory subunit
GPCR	G Protein Coupled Receptor
HEK293T/17 cells	Human Embryonic Kidney 293T/17 cells
IEP	Individualized Education Plan
kB	Boltzmann Constant
MAPK	Mitogen Activated Protein Kinase
MD	Molecular Dynamics
molGRK3ct - Nluc	mas G Protein- Coupled Receptor Kinase 3 C - Terminal fused with NanoLuciferase
MRI	Magnetic Resonance Imaging
Nluc	NanoLuciferase
NMR	Nuclear Magnetic Resonance
NS	Nanoseconds
PI3K	Phosphoinositide 3 - Kinase
PPI	Protein- Protein Interaction

PS	Phosphatidylserine
RMSD	Root Mean Square Deviation
RMSF	Root Mean Square Fluctuation
T	Absolute Temperature
WT	Wild Type
ΔG	Gibbs Free Energy Change
$\hat{H}$	Hamiltonian Operator
τ	Time
Ψ	Wave Function

List of Figures

List of Tables

1. Literature overview

1.1. GNB1-Encephalopathy

GNB1 encephalopathy (GNB1-E) is an extremely rare genetic disorder caused by a point mutation in the GNB1 gene (specifically in the beta 1 subunit) which is inherited in an autosomal dominant manner. Most affected patients carry de novo mutations, but a familial transmission is also possible. Diagnosis of this heterozygous mutation is made through molecular genetic analysis. MRI often reveals cerebral structural abnormalities such as delayed myelination and polymicrogyria (Reva-Politi et al., 2020). To date, fewer than 70 cases of GNB1 have been documented worldwide (www1).

1.1.1. Therapy

Currently there is no causal treatment that promises a cure for the disease. Therapeutic efforts focus exclusively on symptom relief, and in addition collaborative care is needed.

- A combination of occupational and physical therapy that also assists the patients and their families with feeding, especially during infancy, are crucial.
- To guide the patients and their families to show them the importance of improving mobility, so they can regain a piece of quality (Reva-Politi et al., 2020).
- The most common medication that is prescribed are classic anticonvulsants for controlling epileptic seizures; e.g. deep brain stimulation and can be treated with intrathecal baclofen pumps (Nasvytis et al., 2024).

1.1.2. Molecular Pathogenesis

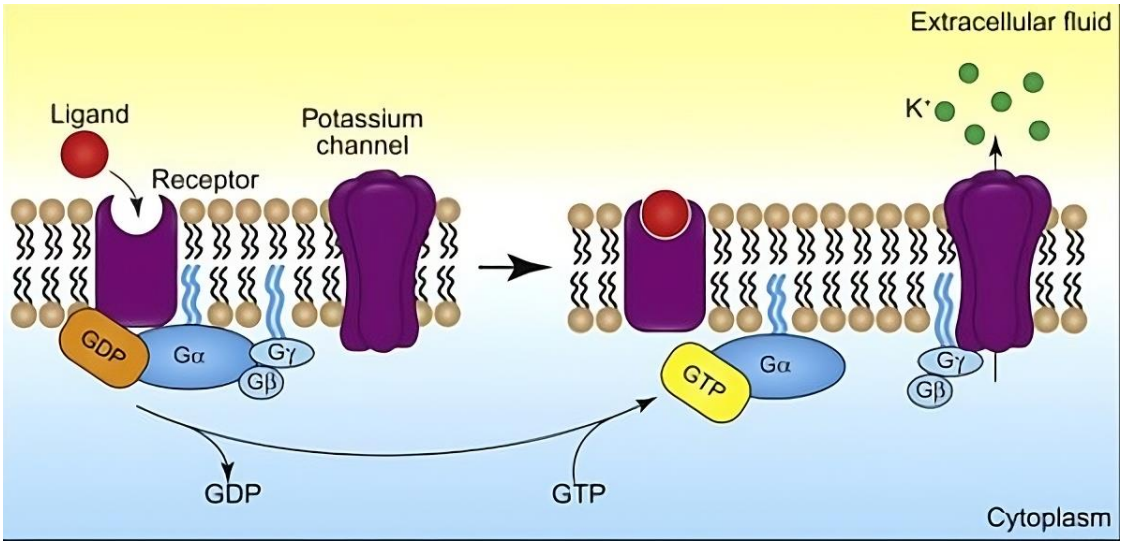

Figure 1: GPCR activation of a GIRK channel (Meriney et al., 2019).

The GNB1 gene codes for the beta 1 subunit of a heterotrimeric G protein that is of immense importance when it comes to signal processing from G protein coupled receptor (GPCRs). Activation of GPCRs causes dissociation of the alpha and beta-gamma subunits, each influencing different intracellular effectors. Gβγ regulates ion channels, phospholipases, and critical signaling pathways such as PI3K. Many pathogenic variants in GNB1 encephalopathy are missense mutations occurring in exons 6 or 7. Interaction between Gβ1 and Gα are significantly destabilized by mutations, and damage severly the cascade through *gain of function, loss of function,* or *dominant-negative* effects that shows that mutations like K78R for example have an increased signal activation (*gain of function*) in mainly affecting neuronal GIRK channels. Mutations like I80T or M101V show a reduction in function *(loss of function*). That means that the pathophysiology of GNB1 encephalopathy originates from mutational alterations affecting the regulation of neuronal ion channels (Reddy et al., 2021).

1.2 Clinical Presentation

GNB1 encephalopathy shows a delay in development with or without cognitive impairments. Aside from the main syndromes, the GNB1 encephalopathy shows secondary symptoms such as muscle tone abnormalities, unusual eye movement and visual disturbance as well as behavioral disorders like autism can be observed. In addition to gastrointestinal issues, cardiovascular anomalies, and urogenital problems can also affect patients' quality of life. Early signs that

parents often notice are feeding difficulties during infancy, and those can progress later into global developmental delays, struggling with the independence of walking that in some cases never happens. Dystonia, myoclonus, or other dyskinesias are often witnessed. When it comes to epilepsy, different types like focal, generalize or status epilepticus can manifest, also West Syndrom in children is a common form of epilepsy (Nasvytis et al., 2024).

1.3 Prognosis

There is no definitive statement about average life expectancy, as most documented cases so far involve children or adolescents. There was one reported death of a child at the age of four, although the exact cause of death could not be determined. Reports indicate that affected individuals can live beyond the age of 18. In rare cases, inheritance is possible. At least four parents have identified who carry a GNB1 mutation, suggesting a milder course of the disease and the potential for transmission. There is also speculation that mutation may influence oncological risk in affected individuals. If medical care is provided properly, a normal life expectancy may be achieved for the patients because those conditions do not come often along with severe congenital organ defects (Reva-Politi et al., 2020).

1.4 Diagnosis and Assessment

According to genetic testing, the foundation of the diagnosis of GNB1 encephalopathy is established; analyses are carried out to understand large scale genetic alterations such as deletions or duplications. Seeing no significant abnormalities, modern sequencing methods are often utilized to specifically examine multiple genes. If there is a suspicion of GNB1 encephalopathy, it normally will present as a combination of moderate to severe developmental delays and neurological or physical abnormalities including: Early-onset muscular hypotonia, Epileptic seizures, Behavioral abnormalities or visual impairments, Gastrointestinal symptoms (Revah-Politi et al., 2020). Diagnostic testing will be launched when pathogenic variants in the GNB1 gene are confirmed.

These tests include:

Blood and cerebrospinal fluid (CSF) analysis: Electrolytes, amino acids, and indicators of metabolic processes evaluate.

EEG diagnostics: Even if the patient is not suffering from epileptic episodes, EEG testing is recommended in both wakefulness and sleep states. Epileptic episodes can cause hypsarrhythmia, slowing brain activity. Looking into that animal models with GNB1 mutations exhibit similar EEG patterns, supporting the role of these mutations in the disease mechanism. Even when there are no abnormalities suspected, it is recommended to undertake MRI imaging to reveal delayed myelination, enlarged ventricles, or malformations of the cerebral and cerebellar cortex (Nasvytis et al., 2024).

1.5 Treatment

Various studies using mature neuronal cell cultures from mice carrying the GNB1 K78R mutation demonstrated that ethosuximide can restore normal neuronal activity. Other medications have also been tested for their effectiveness in treating symptoms: Valproic acid showed inhibitory effects on abnormal neuronal hyperactivity in experimental models and, like ethosuximide, nearly eliminated spike-and-wave discharges following acute treatment (Colombo et al., 2023). The anticonvulsant clobazam was evaluated in a study involving 417 individuals with epilepsy. A year later it shows in the result, that 36% of patients were seizure-free, 18% have demonstrated a reduction in seizure severity meanwhile only 7.7% showed no change (Joshi et al., 2014). Having children that were diagnosed with GNB1 encephalopathy, an Individualized Education Plan (IEP) is recommended in collaboration with a multidisciplinary team including therapists, physical therapists, and educators. The goal is to address learning difficulties, muscular hypotonia, and mobility impairments. That means that they are ensuring the best possible academic and physical participation (Revah-Politi et al., 2020).

2. Gaβγa- Complex, Its Role and Structure

Activation of G proteins occurs upon stimulation of G protein-coupled receptors (GPCRs), which mediate signaling cascades triggered by hormones, neurotransmitters, and other extracellular messengers. Especially these signal pathways control a broad spectrum of cellular

processes. Neuronal transmission, vision, hormone secretion, as well as cell movement and growth are incorporated as a part of these pathways.

Gα, Gβ, and Gγ are the three subunits of the G protein that, in their inactive state, assemble into a heterotrimeric complex. Gα is bound to GDP and maintains the association with the Gβγ dimer, when not active. Upon activation by a GPCR, GDP is exchanged for GTP on Gα, leading to the dissociation of Gα–GTP from the Gβγ dimer. Both Gα - GTP and Gβγ can then interact with downstream effectors to propagate the signal. The Gα subunit is responsible for either activating or inhibiting various intracellular effector proteins such as adenylyl cyclase or phospholipase C, depending on the specific Gα type present. The Gβγ dimer is not only a passive component, but it can also independently activate effector proteins. That results into that Gα re-associating with Gβγ, forming the inactive G protein complex once again. The complex is involved in many essential bioactive processes, such as the regulation of heart rate via sympathetic and parasympathetic signaling. Gβγ, for example, activates the GIRK channel (G protein-coupled inwardly rectifying potassium channel), which is responsible for altering the membrane potential. Its opening allows electrical excitability in cardiac and neuronal cells. The rapid activation of this channel by Gβγ is a key mechanism that translates GPCR signals into a cellular response (Malerba et al., 2019).

The heterotrimeric G protein comprises three subunits: Gα, which is bound to GDP, which acts as a molecular switch, Gβ, and Gγ. While Gα and Gβ are connected through two specific separated contact sites, there is a large interaction surface between the Gβ and Gγ subunits, whereas Gα and Gγ have little direct interaction. The Switch II region between Gα and Gβ plays an important role for these interactions and signaling. Binding of GTP results in regional conformational change, leading to the dissociation of the subunits. Gβ consists of seven WD40 repeats, which form a ring-shaped β-propeller conformation. The inner, protected areas of this structure are functionally flexible. The β-propeller functions as a structural scaffold, with outward-facing loops that facilitate potential interactions. The Switch II interface between Gα and Gβ is essential for signal transduction due to its ability to undergo conformational changes (Wall et al., 1995).

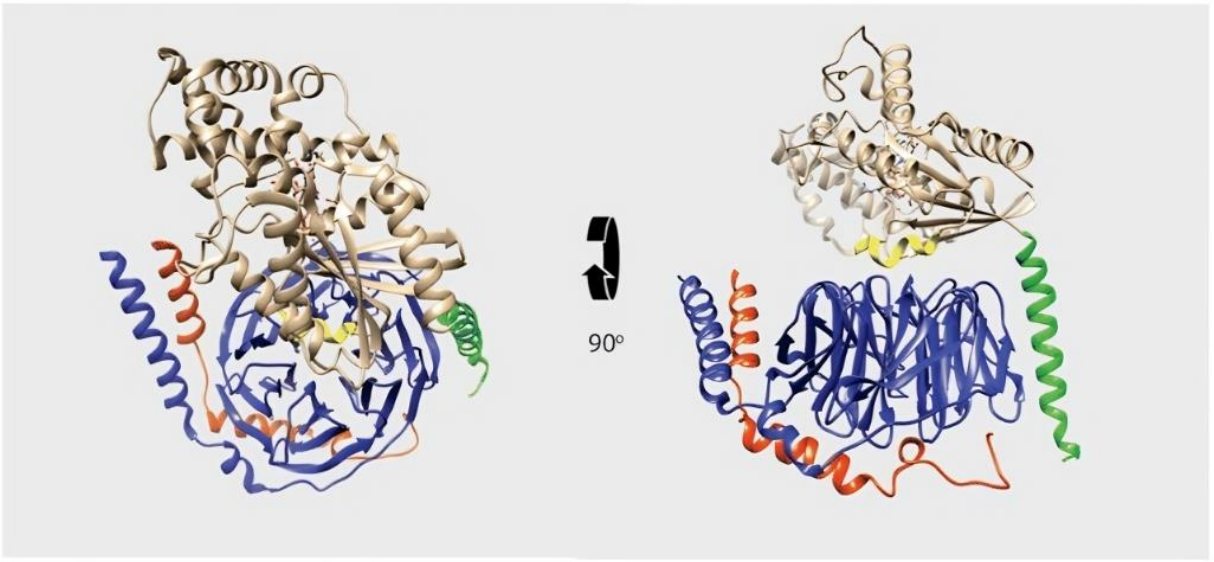

Figure 2: *Ribbon diagram of the heterotrimeric G protein Gαi1β1γ2 (Smrcka et al., 2019).*

The ribbon representation shows the heterotrimeric G protein composed of the Gβ1 subunit (blue), Gγ2 subunit (red), and Gαi1 subunit (green). The switch region within the helical domain of Gαi1, which is involved in conformational transitions during activation is highlighted in yellow (Smrcka et al., 2019).After the agonist binds to the receptor, the GTP-bound Gα subunit detaches from the Gβγ dimer, which plays an essential role in GPCR signaling and is involved in the regulation of various cellular functions. The structure of the Gβγ dimer then comprises seven WD40 repeat "blades," which form a β-propeller structure. The binding between Gγ and Gβ is then moderated by a coiled-coil interaction, resulting in a stable and functional unit. WD40 domains are structurally quite set and do not allow significant conformational changes upon dissociation from Gα. Blades 1 till 4 of the Gβ subunit are understood as the main interaction surfaces for Gα and downstream effectors. In terms of function the dissociation of the Gβγ dimer represents a significant regulatory step in several cellular signaling pathways (Chung et al., 2021).

2.1 G64V Pathogenic Variant

De novo missense mutation in the GNB1 gene were observed in 13 patients with developmental delays, muscle weakness, and epileptic episodes. The causes of these diseases are often due to mutations in specific regions of the GNB1 gene. GNB1 encodes the beta 1 subunit of the G protein, which plays a central role in signal transduction. As a result of this alteration, malfunctions in activation or reduced binding affinity to effectors may occur, which interferes with

normal signal transmission. Clinically affected patients show global developmental delay, muscle weakness, epileptic seizures, and also physical retardation (Petrovski et al., 2016). It is currently known that regional mutation hotspots (49% out of the patients) are located between exon 6 and exon 7, which represent a major part of the identified missense mutations. In silico modeling shows that these mutations affect the WD40 domains of the protein. This region is of great importance when it comes to signal transduction in cooperation with other G protein components. This highlights the wide range of symptoms associated with GNB1 encephalopathy and that's what provides valuable insight for future research and potential treatment on affected individuals (Da Silva et al., 2021).

The focus of this work will be the G64V mutation.

Table 1.

Clinical, genetic and functional information of mutation carriers

Case	1	2	3	4	5	6	7	8	9	10	11	12	13	14	15	16
Sex	M	F	F	M	M	M	F	M	F	F	M	M	F	M	F	M
Age at diagnosis	4	2.5	4	2.4	5	8	2.9	4	6	1	Unk	8	12	8	6	8
Ethnicity	Saudi Arabian	Qatar	Egypt	Saudi Arabian	Israeli	Mexican	Saudi Arabian	Kuwaiti	Israeli	Indian	Mexican	Algerian	German	Saudi Arabian	Indian	Saudi Arabian
Var Build 19	1:1749284	1:1747244	1:1747207	1:1736021	1:1736013	1:1736016	1:1736014	1:1736008	1:1736001	1:1736001	1:1736001	1:1735972	1:1735935	1:1720492	1:1718877	1:1718784
NM 002074	c.88C>T	c.154C>G	c.191G>T	c.268-1G>T	c.272_275del	c.272A>G	c.274G>A	c.280C>T	c.287G>T	c.287G>T	c.287G>T	c.316G>A	c.353A>G	c.915_916del	c.917-1G>T	c.1009A>C
NP 002065	p.L30F	p.R52G	p.G64V	p.?	p.?	p.H91R	p.A92T	p.P94S	p.R96L	p.R96L	p.R96L	p.A106T	p.D118G	p.?	p.?	p.K337Q
Location of mut.	Exon 4	Exon 5	Exon 5	Intron 6	Exon 7	Exon 7	Exon 7	Exon 7	Exon 7	Exon 7	Exon 7	Exon 7	Exon 7	Exon 10	Intron 10	Exon 11
Type of mut.	ms	ms	ms	ss	fs	ms	ms	ms	ms	ms	ms	ms	ms	fs	ss	ms
Change in function	No	Yes	Yes	Not tested	Not tested	No	Yes	Yes	Yes	Yes	Yes	Yes	Yes	Not tested	Not tested	No
CADD score (v1.3)	22	21	33	27	35	18	25	23	26	26	26	24	29	35	26	24
Inheritance	*De novo*	*De novo*	*De novo*	*De novo*	*De novo*	Unk	*De novo*	Unk	Dominant	Dominant	Dominant	*De novo*	*De novo*	*De novo*	Unk	*De novo*
GDD	No	Yes	Yes	Yes	Yes	Yes	Yes	Yes	Yes	Yes	Yes	Yes	Yes	Yes	Yes	Yes
Growth delay	Yes	No	No	No	Yes	Yes	No	No	Yes	No	No	No	No	No	Yes	No
Muscular hypotonia	Yes	No	No	Yes	No	Yes	Yes	No	No	No	No	No	Yes	Yes	Yes	No
ID	Yes	Yes	No	Yes	Yes	Yes	Yes	Yes	No	Yes	Yes	No	Yes	Yes	Yes	Yes
Seizures	Yes	No	No	No	Yes	Yes	Yes	No	Yes	No	Yes	Yes	No	Yes	Yes	Yes
Craniosynostosis	No	No	No	Yes	Yes	No	No	No	No	No	No	Yes	No	No	No	No
Cerebellar hypoplasia	No	Yes	No	No	No	Yes	Yes	No	No	No	No	No	No	No	No	No
Abnormal myelination	No	No	No	Yes	Yes	No	No	No	Yes	No	Yes	No	No	Yes	No	Yes
Ophthalmoplegia	No	Yes	No	Yes	No	No	No	Yes	Yes	No	No	No	No	No	No	No
Nystagmus	Yes	Yes	No	No	Yes	Yes	No	No	Yes	No	Yes	No	No	Yes	Yes	Yes
Ataxia	Yes	Yes	No	No	Yes	No	Yes	No	No	No	No	No	No	No	Yes	No
Chorea	No	No	No	No	No	No	No	Yes	No	No	No	No	No	No	No	No
Dystonia	No	No	No	No	No	No	No	No	No	No	No	No	Yes	No	No	No

Unk, unknown; ss, splice site; fs, Frameshift; ms, missense; GDD, global developmental delay; ID, intellectual disability; CADD, combined annotation dependent depletion.

Figure 3: *This table summarizes clinical, genetic, and functional information on patients carrying GNB1 mutations, including the patient carrying the G64V variant (marked in blue) (Lohmann et al., 2017).*

In this table, various point mutations and their respective regions were observed; for example the exon in which the mutation is located, the mutation type, as well as a selected list of the most prominent symptoms that a point mutation in *GNB1* can cause, such as GDD (Global Developmental Delay), growth retardation, muscle weakness, and others. According to the table, the patient carrying the G64V mutation is of Egyptian origin and was

diagnosed at the age of four. This mutation is a missense mutation and occurs as a de novo event, meaning that neither parent carries the mutation nor passed it on to the child. This contrasts with, for example, the R96L mutation, which is transmitted through an autosomal dominant mechanism in three reported cases. The missense mutation observed in G64V leads to a loss of function. Other types of mutations, such as splice site or frameshift mutations, are also categorized as pathogenic, as they can similarly result in loss of function (Lohmann et al., 2017). Based on Stefl et al. (2013) the definition of a missense mutation is a variation in a single nucleotide in the DNA. Replacement of one amino acid for another is the main cause. As a result, a different amino acid is incorporated into the protein than originally intended. This alters the three-dimensional structure of the protein. The stability and dynamics of the protein, along with changes to its surface properties, can weaken its ability to interact with other molecular structures. This leads to a loss of normal protein function, leading to disease (Stefl et al., 2013). Glycine is a polar and hydrophilic amino acid with no side chain, just a hydrogen atom. It is one of the smallest amino acids and frequently occurs in proteins. Valine, on the other hand, is a non-polar, hydrophobic amino acid with a side chain and is significantly larger than glycine (Breimann et al., 2024).

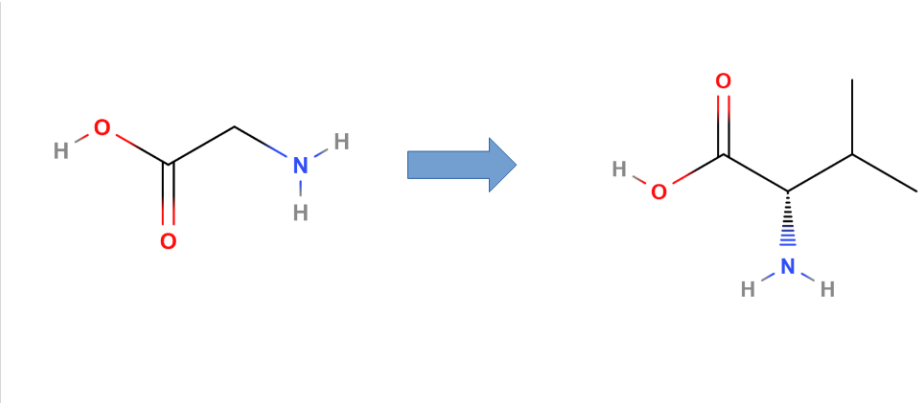

Figure 4: *Substitution of glycine with valine. Created using MolView. MolView (www2) was used to create this figure.*

In the Lohman studies (Lohmann et al., 2017) 14 new mutations were identified through exome sequencing, including 10 missense mutations. Further functional tests were conducted to investigate signal transduction as well as protein complex formation in these mutations. The ability of involvement of G protein subunits, Gαolf and Gγ2, to trigger a signaling cascade was investigated by using the so-called BRET method. BRET (Bioluminescence Resonance Energy Transfer) labels proteins with fluorescent markers, and the interaction can be detected by measuring emitted light. This is how it's been shown to efficiently assess the pathogenicity of versions in the GNAL gene, which carry the information for the Gαolf subunit. The signal

transduction for D1 dopamine receptor is involves the Gαolfβ1γ2 complex, where pathogenicity is linked to symptoms of dystonia (Lohmann et al., 2017). The principle of BRET is the energy transfer from a labeled protein, called the BRET donor, to the BRET acceptor. This energy transfer generates a signal that represents the interaction between the two (Vickers et al., 2016).

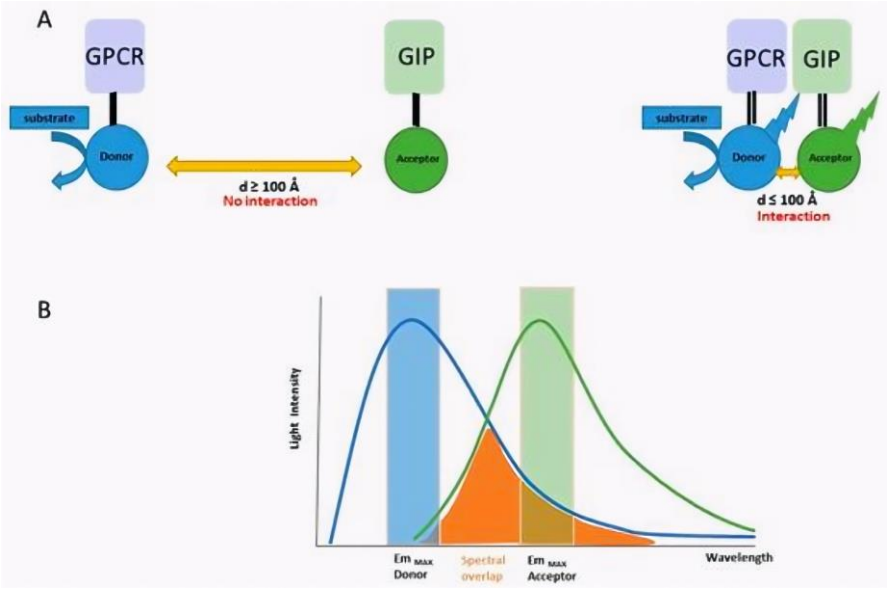

Figure 5: *BRET Scheme. (A) This illustrates the ability to detect the interaction between a GPCR and its interacting protein (GIP). (B) The generation of a BRET signal is based on the interaction between the donor and the acceptor: the donor's emission spectrum must intersect with the excitation spectrum of thee acceptor to allow energy transfer and therefore BRET to occure (El Khamilchi et al., 2019).*

The upside of BRET is that it doesn't need an external light source and is subject to few interfering factors. It also allows BRET analysis in living cells. BRET is often used for GPCRs and can visualize interactions with other molecules. For example, this method has been applied to visualize receptor dimerization (dopamine D2 and TAAR) and in drug screening research (Salahpour et al., 2012).

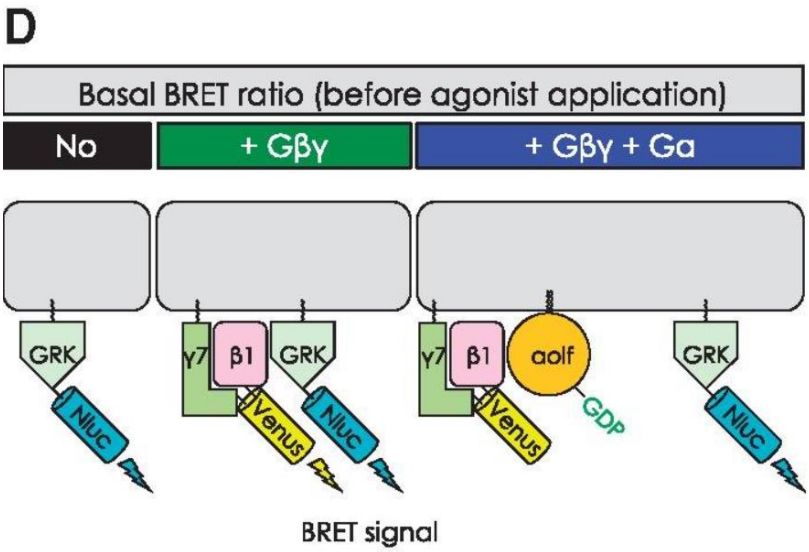

Figure 6: *Schematic illustration of the basal BRET signal is and its determination (Lohmann et al., 2017).*

Through the transfection of masGRK3ct-NLuc, which was labeled with an Nluc marker, and Venus-Gβ1γ7, which was tagged with the Venus marker, a BRET signal is generated when both proteins interact. If the alpha subunit is additionally expressed, the BRET signal will be reduced due to trimer arrangement. The effects of the 10 GNB1 missense mutations on the dopamine D1 receptor via the Gαolfβ1γ7 complex were investigated. Using BiFC, it was examined whether the mutation-altered β1 proteins can form stable dimers with the Gγ7 subunit (Lohmann et al., 2017).BiFC (short for bimolecular fluorescence complementation) is a method used to detect and understand protein–protein interactions in living cells. In principle, two separated fragments of fluorescent proteins are put together when the attached proteins interact with each other (Kerppola et al 2008). Venus is a modified form of yellow fluorescent protein that is used in BiFC methods to detect interactions between proteins, as shown in the study by Ohashi, for example (Ohashi et al., 2012).

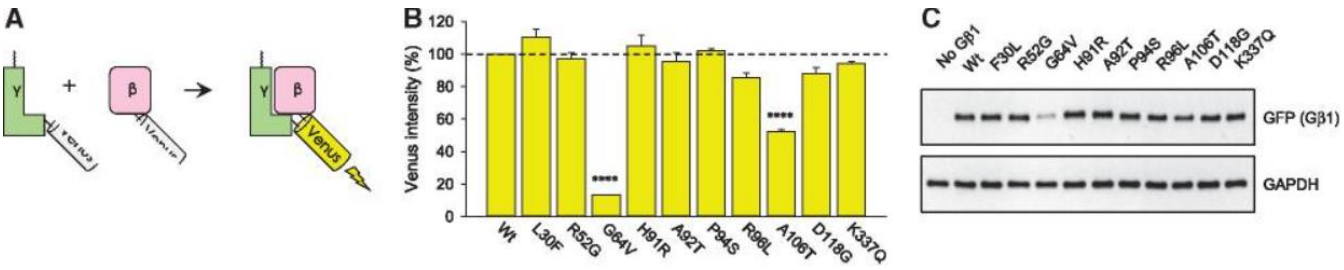

Figure 7*: Schematic of Venus-based Gβ1/Gγ7 dimerization (A), fluorescence quantification of wild type and G64V mutant (B), and corresponding Western blot analysis showing impaired expression of G64V (C) (Lohmann et al., 2017).*

In Figure 7 from the Lohmann study (2017), schematic illustration **A** visually shows how the subunits Gγ7 and Gβ1 are separately bound to different parts of the Venus protein. As soon as the fusion of the two subunits occurs, the Venus protein fluoresces, therefore its indicates the successful binding of both subunits. In graph **B**, the evaluation of the dimerization of the subunits is shown for the wild type (WT) and various mutations, including G64V, which are listed on the X-axis. On the Y-axis, the fluorescence intensity of the Venus protein is shown. The stronger the dimerization between the subunits, the higher the Venus fluorescence intensity. It is clearly visible that G64V shows a very weak Venus signal, which indicates poor dimerization. Experimentally, HEK293T/17 cells were transfected for a defined period with the D1 dopamine receptor (D1R), Gαolf, Venus-156-239-Gβ1, Venus-1-155-Gγ7, and an effector reporter (masGRK3ct-Nluc). In panel **C**, the result of a Western blot is shown, which displays protein expression. For this, the same cell lysates were used as in the Venus fluorescence intensity analysis shown in panel B. Anti-GAPDH antibodies were used as a control to ensure equal total protein levels in all samples. Anti-GFP antibodies were applied to identify fusion proteins. Again, it is noticeable that G64V shows no signal, suggesting a reduced level of expression. (Lohmann et al., 2017).

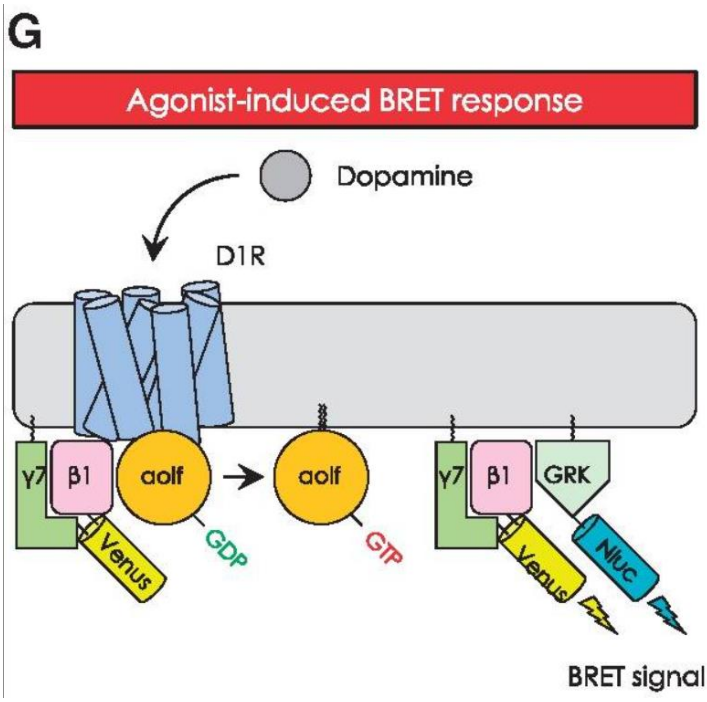

Figure 8: *Agonist induced BRET response triggered by the ligand dopamine (Lohmann et al., 2017).*

This schematic illustrates how the G protein is activated by the binding of an agonist, in this case dopamine. As a result, Gαolf separates from the Gβ1γ7 subunit, which then bind to masGRK3ct-NLuc, triggering a BRET signal (Lohmann et al., 2017).

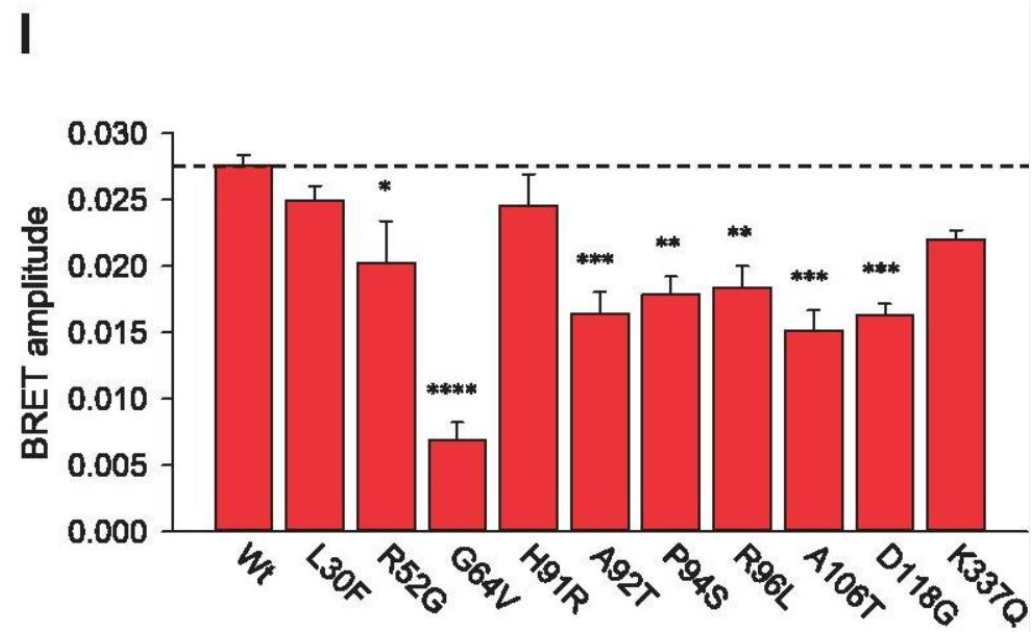

Figure 9: *BRET amplitude with dopamine agonist showing reduced signaling for G64V mutation (Lohmann et al., 2017).*

Related to Figure G, this graph shows the BRET amplitude results in response to the addition of the dopamine agonist for the respective mutations. As seen before, the missense mutation G64V again exhibits low signaling, indicating impaired Gβγ binding (Lohmann et al., 2017).

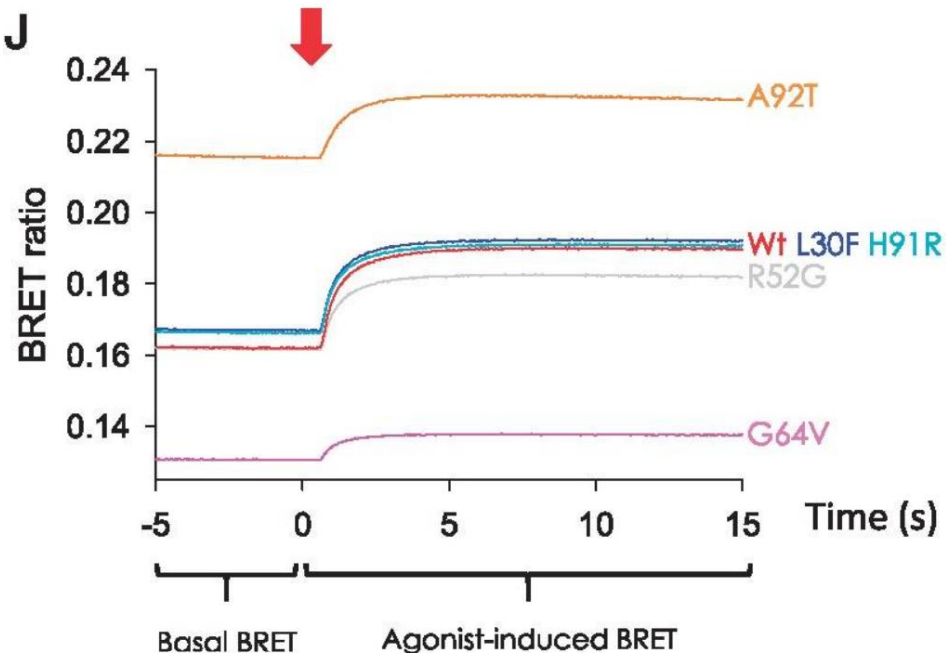

Figure 10: *Dopamine-induced BRET signals showing reduced response for G64V mutant (Lohmann et al., 2017).*

The x-axis of the portrays time courses shows the chronological progression of both basal and agonist-induced BRET signals for the wild type (WT) and the Gβ1 mutants. The red arrow marks the time point of dopamine application (100 µM), which activates the D1R and triggers the dissociation of Gαolf from the G-protein trimer. As a result of this an increase in the BRET signal is observed. The curves represent the mean of six experimental replicates. As seen in other figures, the G64V mutation shows a very low BRET ratio, again indicating an impaired activation process of the G protein by the receptor (Lohmann et al., 2017).

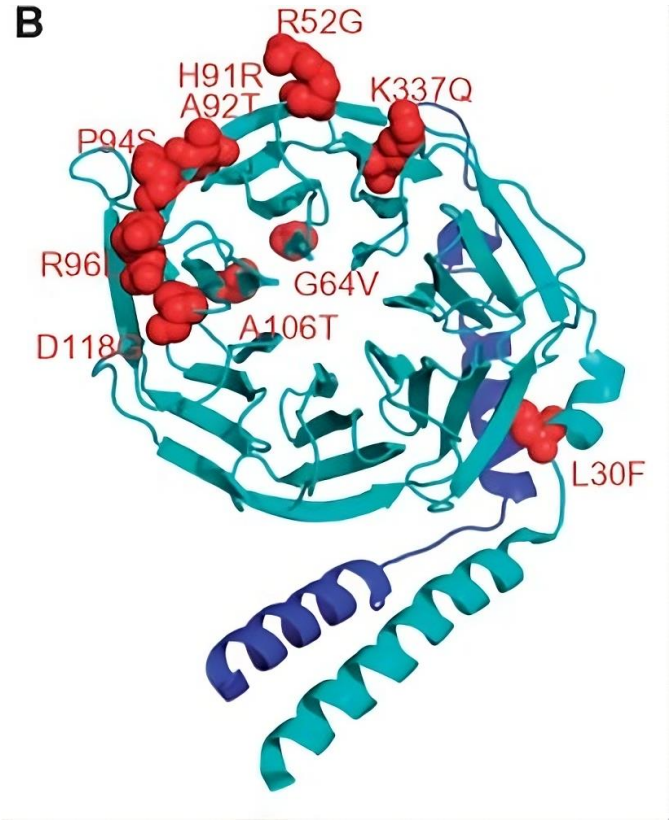

Figure 11: *All disease associated mutant residues in the Gβ1γ2 dimer, including the G64V substitution, are highlighted in red (Lohmann et al., 2017)*

Regarding the functional impairments caused by GNB1 missense mutations, splice site and frameshift variants have been classified as disease causing, leading to loss of function in the protein. Previous analyses using BRET and BiFC show problems with the dimerization of Gβ1 and Gγ2, especially in G64V, which leads to complicated protein folding. The average age at diagnosis of GNB1 mutations is 5 years (Lohmann et al., 2017).

3. From Quantum Mechanics to Molecular Dynamics

MD simulations rely on certain assumptions to represent systems, which ideally would be described by quantum mechanics, using classical models. Ideally such complex processes could be described by the time dependent Schrödinger equation for many particles with interacting electronic states, but this is not practical for systems with a large number of electrons (Ojanperä et al., 2012).

$$\hat{H}\Psi_n = i\hbar\frac{\partial\Psi_n}{\partial t}$$

Ψ denotes the wave function of the system in state n, $\partial/\partial\tau$ is the partial rate of the change regarding time. Ĥ stands for the Hamiltonian operator, indicating the entire energy of the system, consisting of both kinetic and potential energy. According to Atkins et al. (2017), the Schrödinger equation cannot be solved exactly for molecules due to the presence of multiple interacting particles. The Born Oppenheimer approximation is since nuclei have a much greater mass than electrons and that's why they move significantly more slowly. As a result, the nuclei can be considered stationary relative to the electrons. Under this approximation, the total wave function of the system can be separated into a nuclear and an electronic component (Atkins et al., 2017).:

$$\Psi(r,R) = \chi(R)\psi(r;R)$$

Here, Ψ is the total wave function of the system, with r representing the electronic coordinates, R the nuclear coordinates, and time t. $\psi_n$uc is the nuclear wave function, and ψ_{el} is the electronic wave function that depends parametrically on the fixed positions of the nuclei (Atkins et al., 2017).

The Born–Oppenheimer approximation equation shown above separates electron and nuclear motion with the electronic structure calculated for a fixed nuclear configuration. Electrons are in the ground state and adapt to nuclear motion. The electronic structure is calculated separately for each nuclear configuration, and the energy is used to calculate the forces on the nuclei. The nuclear motion follows Newton's law classically (Ribaldone et al., 2024).

$$F_i = m_i\frac{d^2r_i}{dt^2}$$

Newton's Equation of motion

Ehrenfest MD, as described by Andrade (2009), allows electronic states to exist in superposition, unlike Born–Oppenheimer MD which only considers the ground state. The method is based on the separation of electronic and nuclear motions. The short time steps in Ehrenfest MD enable capturing electronic frequencies (Andrade, 2009).

3.1 Molecular Dynamics Simulations

Molecular dynamics (MD) simulations are essential methods in various research fields, enabling computer generated insights into structures state that can otherwise be complicated to study. Simulations can be run over multiple days, providing precise results and they also deliver insights into receptor-ligand structures as well as their dynamics and kinetics. The latest MD studies can simulate macromolecules over milliseconds and even longer time periods. MD simulations have also taken an important role in drug development by improving the understanding of structures and functions of GPCRs.Three important points for an MD simulation: Modeling system, a force field, simulation software such as Amber, CHARMM, GROMACS, or NAMD (Zou et al., 2019). Methods like X-ray crystallography, NMR, or Cryo-EM have been able to show the resolution of many protein structures. However, some proteins remain structurally uncharacterized because structural biology techniques usually provide snapshots and can't show dynamic processes on a molecular level. Therefore, detecting molecular movements and conformational changes is important. MD complements experimental approaches (Kameda et al., 2022).

According to De Vivo et al., 2016, computer-aided drug discovery is increasingly becoming a standardized method. MD considers molecular flexibility and disorderly effects. Advances in hardware and software make simulations possible within a practical timeframe making MD routine in structure based drug design (SBDD): MD is based on classical Newtonian physics, where forces are described by force fields. Classical molecular dynamics describes, according to Newtonian mechanics, the motion and interactions between atoms and molecules. Forces between particles are calculated via force fields that determine the energy balance of the overall system. The position and also velocity of particles are recorded as so-called trajectories or system states, which are derived from equations of motion. From these, physical properties such as free energy, kinetic constants, and other parameters can be derived and compared to experimental data. MD simulations were originally developed for theoretical physics in the early 1950s but have since found their importance in the field of chemistry and drug discovery (De Vivo et al., 2016).

3.2 Thermodynamics and Free Energy

To illustrate biological processes of proteins such as folding or formation, the thermodynamic and kinetic behavior of a system is described. For example, protein in solutions can either occur in undefined states or in well distinct secondary and tertiary structures. The energy of state A (unfolded) as well as state B (folded) then explains the equilibrium relationship of free energy (Aldeghi et al., 2019).

$$\Delta G = G_A - G_B = -k_B T \, ln \, \frac{p_B}{p_A}$$

The free energy, which encompasses the total phase space of the system, is denoted by ΔG under isothermal isobaric conditions. As mentioned before, GA describes the unfolded state of the protein, while GB represents the folded state. β = 1/kBT, where kB is describing the Boltzmann constant and T stands for the absolute temperature. This indicates that the change in ΔG sets an upper limit on the work. So this can be generated in an isolated system under reversible conditions. A difference is made between a reversible process in the system and a process within a finite time interval.

In a reversible process, thermodynamic equilibrium exists, and processes proceed infinitely slowly (Aldeghi et al., 2019). In a finite time interval, however, the system is no longer in equilibrium, which leads to temperature loss and converts the process from reversible to irreversible. Based on the second law of thermodynamics, the standard work expended usually exceeds the energy difference because the irreversible behavior causes a dissipative energy loss (Aldeghi et al., 2019).

$$\langle W \rangle (\tau) \langle \geq \rangle \Delta G$$

3.3 Free Energy Changes and their calculations based on Amino Acid Mutation (ΔΔG)

Through point mutations in amino acids (amino acid mutations), the free energy changes, which can then be illustrated with MD simulations. The prediction of the shift in free energy upon mutations is an important aspect of protein engineering research. This improves the

understanding of drug resistance development. In a finite-time process, the performed work can be calculated by integrating over the control parameter (Aldeghi et al., 2019).

$$W(\tau) = \int_0^1 \frac{\partial H(x, v, \lambda)}{\partial \lambda}, \, d\lambda$$

Here, H denotes the Hamiltonian function, which represents the energy state of the system and is influenced by the positions, velocities v, the control parameter λ, and the phase space x (Aldeghi et al., 2019).

According to Jarzynski's equality, the free energy difference ΔG can be determined using the exponential average of the performed work:

$$\langle e \rangle^{-\beta W(\tau)} \langle = \rangle e^{-\beta \Delta G}$$

This approach (Jarzynski's equality) is however often error prone, because rare trajectories with low energy dissipation strongly influence the estimate and because of slow down convergence. This equation also only describes transitions in one direction (λ = 0 to λ = 1) (Aldeghi et al., 2019).

The Crooks fluctuation theorem whatsoever considers transitions in both directions, namely forward and reverse. The probability distributions of the processes are related to work W and the free energy difference ΔG as follows (Aldeghi *et al.*, 2019):

$$\frac{P_f(W)}{P_r(-W)} = e^{\beta(W-\Delta G)}$$

According to the Crooks fluctuation theorem, the forward and reverse work distribution gives information about the free energy difference. Should they overlap sufficiently, the point of intersection indicates ΔG. $P_f(W)$ and $P_r(-W)$ stand for the work distributions of the forward and reverse processes, respectively (Aldeghi *et al.*, 2019).

$$\Delta G = W + k_B T \, ln \, \frac{P_r(-W)}{P_f(W)}$$

If both distributions intersect, then ΔG = W. If the overlap is small, the method becomes very sensitive and the precision of the distribution decreases. However, the work distribution can be approximated using so called Gaussian curves. The Crooks Gaussian Intersection (CGI) method provides more accurate and stable values for free energy:

If the forward and reverse distributions intersect then $\Delta G = W \Delta G = W \Delta G = W$. The Crooks Gaussian Intersection (CGI) method provides a more accurate estimation:

$$\Delta G = \frac{\sigma_f^2 + \sigma_r^2}{\sigma_f^2 \langle W \rangle_f \langle - \rangle \sigma_r^2 \langle W \rangle_r \langle + \rangle 2 k_B T \ln \frac{\sigma r}{\sigma_f}}$$

Here, W_f and W_r represent the mean work of the forward and reverse processes, while σf^2 and σr^2 denote the variances of the respective distributions. Another way to estimate free energy differences is the so-called BAR estimator (Bennett's Acceptance Ratio). This method uses the data from both forward and reverse processes (state A and state B) to obtain an estimate. Integrating forward and reverse distributions of the potential energy differences, based on Benette, this gives an accurate estimate of free energy. In nonequilibrium processes, the value ΔU is replaced by W for work (Aldeghi et al., 2019).

$$\sum_{i=1}^{N_f} \frac{1}{1 + \left(\frac{N_r}{N_f}\right) e^{\beta (W_i - \Delta G)}} = \sum_{j=1}^{N_r} \frac{1}{1 + \left(\frac{N_f}{N_r}\right) e^{-\beta \left(W_j - \Delta G\right)}}$$

The BAR estimator can provide unbiased results for a big sample size. It is important that the work values are statistically independent. If too many starting points are chosen too close to each other from the equilibrium simulation, correlations can form and certainly twist the result. The number of forward trajectories is denoted by Nf , whereas Nr corresponds to the number of reverse trajectories (Aldeghi et al., 2019).

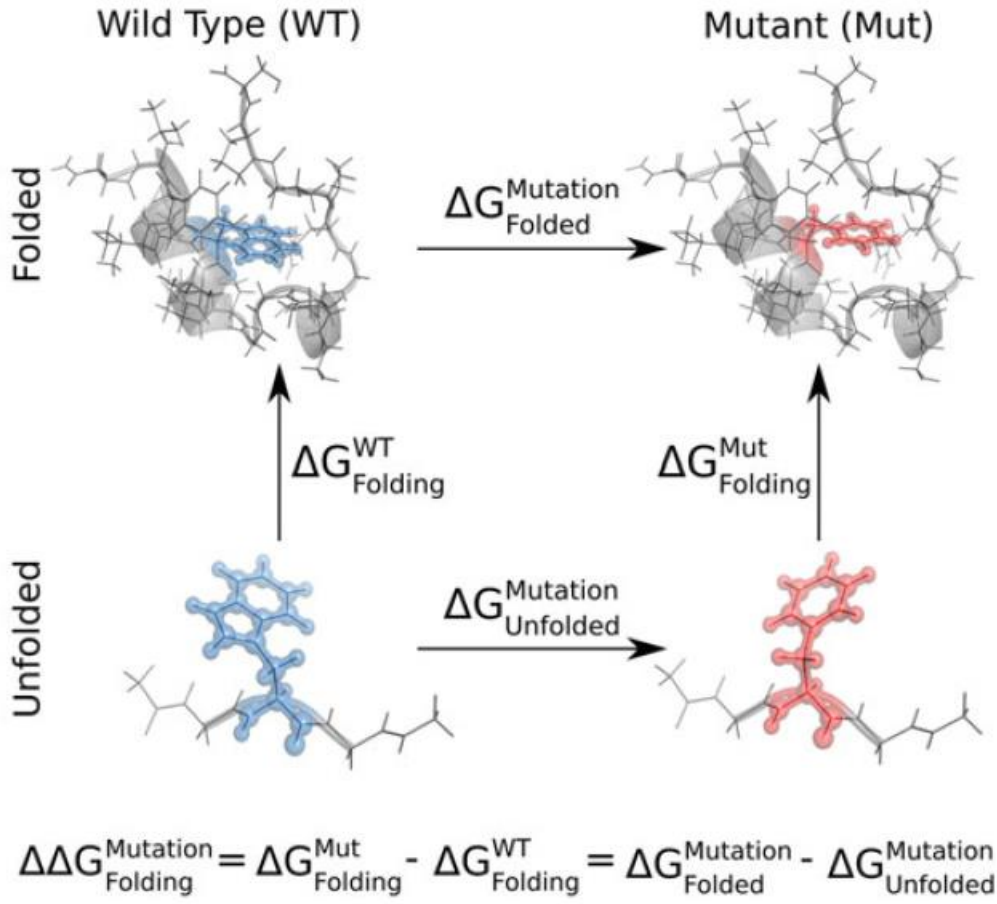

Figure 12: *Thermodynamic cycle scheme for evaluating the change in folding free energy upon mutation* $\Delta\Delta G^{(Mutation)}_{Folding}$. *The cycle links the folding of wild-type and mutant proteins* $\Delta G^{(WT)}_{Folding}$, $\Delta G^{(Mut)}_{Folding}$ *with alchemical transformation in the unfolded and folded states* ($\Delta G^{(Mutation)}_{Unfolded}$, $\Delta G^{(Mutation)}_{Folded}$) *(Aldeghi et al., 2019).*

To determine a free energy difference, the initial and final states must first be established. Then, a transition between the two states is specified. In the case of protein folding, the starting point is the unfolded protein, as the final state indicates the folded protein. The resulting free energy difference represents the energy that is either consumed or released during the folding process. In Figure 12 the thermodynamic cycle is shown is used to determine the change in the protein's folding energy because of a mutation $\Delta\Delta G^{(\text{Mutation})}_{\text{Folding}}$. The vertical branches of the cycle correspond to the physical folding processes of the wild-type and mutant proteins. The left side illustrates the folding of the wild type of protein (WT), which is linked with the free folding energy $\Delta G^{(\text{WT})}_{\text{Folding}}$. On the right side, the same folding process is depicted for the mutated protein, with its corresponding free folding energy $\Delta G^{(\text{Mut})}_{\text{Folding}}$(Aldeghi et al., 2019).

Looking deeper into it, we see that the lower row of the cycle describes an alchemical change: the unfolded wild type protein is converted into the mutated variant, resulting in an energy difference $\Delta G_{\text{Unfolded}}^{(\text{Mutation})}$. The upper row represents the same mutation applied to the folded state of the protein, generating $\Delta G_{\text{Folded}}^{(\text{Mutation})}$. The alchemical transformation shown as the horizontal equation is computationally less demanding, which allows the determination of $\Delta G_{\text{Folded}}^{(\text{Mutation})}$. This value is obtained from the difference between $\Delta G_{\text{Folded}}^{(\text{Mutation})}$ and $\Delta G_{\text{Unfolded}}^{(\text{Mutation})}$ (Aldeghi et al., 2019).

3.4 $\Delta\Delta G_{Folding}^{(Mutation)} = \Delta G_{Folded}^{(Mutation)} - \Delta G_{Unfolded}^{(Mutation)}$

If the 3D structure of the protein under investigation is established, it can theoretically be unfolded by dissociating the molecule apart from the N- to the C-terminus, and the work done during this process can be quantified. Since this method causes structural changes, it is associated with high computational cost. Therefore, the change in folding energy caused by a mutation $\Delta\Delta G^{(\text{Folding})}$can be calculated more efficiently by using a thermodynamic cycle. Computationally, the wild type (WT) is transformed into the mutant (MT) in both the folded and also unfolded states, which achieves faster convergence. Since free energy depends only on the initial and final states, this computational path can be used without losing accuracy. Alchemical mutations are computationally more efficient than physical unfolding, because free energy is path-independent and can thus be calculated via non-physical pathways. Applying the thermodynamic cycle allows an estimation of the modification in folding energy caused by a mutation. The wild type is computationally transformed into the mutant once in the folded and once in the unfolded state. Because the fully unfolded state is difficult to simulate, short peptides such as GXG tripeptides are commonly used as models that approximate the unfolded state well. On the other hand, the folded state, the energy values are already known, so only the mutation energies in the unfolded state remain to be determined. This framework is also useful for studying and describing protein ligand and protein DNA binding (Aldeghi et al., 2019).

4. Objective

The aim of this master's thesis is to evaluate the effect of G64V mutations of the Gβ1 subunit on the stable Gβ1γ2 complex using molecular dynamics. The GNB1 encephalopathy results from a point mutation (G64V) in the beta subunit of the G protein, which impairs signal transduction. Epilepsy, ADHD, autism, gastrointestinal problems, as well as cardiovascular abnormalities belong to the broad spectrum of symptoms of this rare disease. The MD simulations applied here aim to show the consequences of the G64V point mutation on the structure of the G protein and its ability to transmit signals. The initial model was created using CHARMM-GUI, based on PDB 4KFM, to specifically integrate the G64V mutation into the G protein complex with the beta subunit (Gβ1γ2). Short MD simulations were then performed, first on tripeptides and later large protein molecules with Gβ1γ2 subunits. The simulations were subsequently repeated five times for both the WT and the MT. The calculation of the free energy change was the next step, investigating how the MT affects the system energetically to obtain initial indications of possible changes in the stability and potential interactions of the protein. As a final step, the simulation was extended to a total of 250 ns, allowing more trajectories to be analyzed. The dynamics can be analyzed through RMSD and RMSF values, are an important part of understanding the potential changes in protein properties caused by the mutation.

5. Materials and Methods

5.1 Simulation Software and Tools

With technological advancements, numerous specialized programs (software) for computer simulations, such as MD simulations, have been developed. In research, particularly in molecular dynamics, GROMACS, AMBER, CHARMM, and NAMD have become established (Abraham et al., 2015). GROMACS has been especially effective in nanomedicine, and it also provides a wide range of computational methods for molecular systems, making it ideal for analyzing complex biological structures (Xu et al., 2023).

For this master's thesis, GROMACS version 2022.3 with the AMBER99SB*-ILDN force field were used.

5.2 MD Simulation Protocols

The system was placed in a cubic box, solved with the explicit TIP3P water model and then electrically neutralized by adding up a 0.150 M solution of sodium and chloride ions (Hassan et al., 2022). The system undergoes energy minimization to eliminate unfavorable atomic interactions and obtain a stable starting configuration which is also followed by solvation and an equilibration phase with NVT (Number of Particles, Volume, and Temperature) and NPT (Number of Particles, Pressure, and Temperature) ensembles to create realistic conditions in the simulated system. Each equilibration step lasts 100 picoseconds (ps), during which pressure and temperature are monitored until they reach stable values. Subsequently, a production MD simulation of 10 ns is performed. This phase is utilized to characterize realistic molecular motions and dynamics over longer timescales. In this phase, data for the main analysis are collected, such as calculations of energy, conformational changes, or binding interactions. The first 2 ns of the production simulation are discarded as adaptation time, and the remaining 8 ns are used to extract 100 frames at equal intervals of 80 ps. These frames served as starting points for subsequent non-equilibrium transition simulations. The work performed during the phase transition between the two states (WT to MT) was recorded. According to the provided data, the free energy difference between the two states was evaluated with the Crooks fluctuation theorem (Hassan et al., 2022). To accurately determine the free energy, the BAR method (Bennett's Acceptance Ratio) was applied (Reinhardt et al., 2021). A total of five runs were performed for both the protein and the tripeptide systems. Run1 was extended to 250 ns for generating a long-term MD simulation At the end, structural deviations (RMSD) and flexibility of individual residues (RMSF) were analyzed using GROMACS. RMSD (Root Mean Square Deviation) evaluates on how much the protein structure is changing over time compared to a reference structure (Torrens-Fontanals et al., 2020). RMSF (Root Mean Square Fluctuation) shows how many individual residues in the molecule move during the simulation, providing insight into their flexibility (Case et al., 2005).

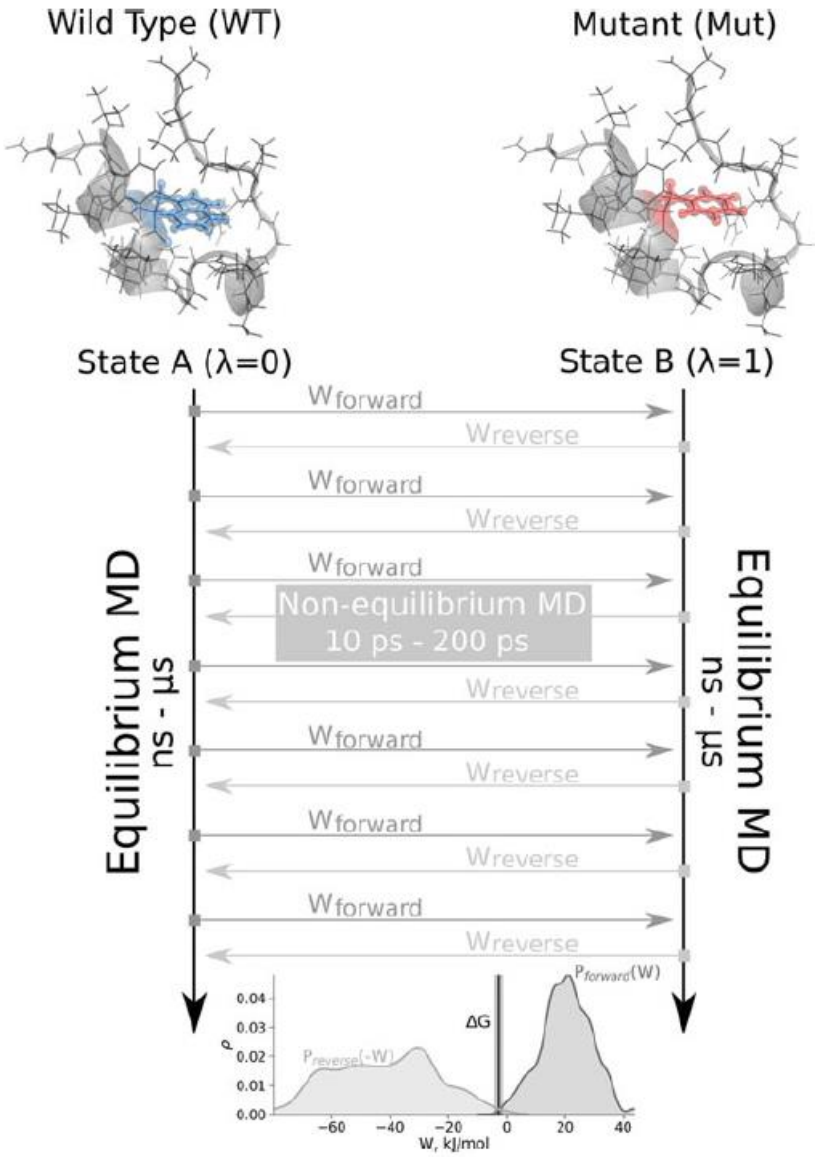

Figure 13*: Equilibrium simulations of WT (λ = 0) and Mutant (λ = 1) with snapshots driving short non-equilibrium transitions to calculate ΔG (Aldeghi et al., 2019).*

In Figure 13 is approach the of two separate equilibrium simulations: the wild-type – State A (λ = 0) and the mutant – State B (λ = 1). It is important that those two simulations are run for a certain period (in the range of nanoseconds to microseconds). From these trajectories, we take snapshots, which then serve as starting points for fast non-equilibrium transitions: for the forward direction (λ: 0 → 1) and on the other hand for the reverse direction (λ: 1 → 0). The transitions last between 10 and 200 ps. During these transitions, work was registered, and using these measured work values, the free energy difference ΔG between wild-type and mutant is afterwards estimated with the Crooks fluctuation theorem (Aldeghi et al., 2019).

6. Results

The results indicate that the G64V mutation contributes to the pathology of GNB1 encephalopathy and exerts its effect within the Gβ1γ2 subunits. To systematically examine this effect, MD simulations were employed to capture both structural and dynamic changes. Data was obtained from the Protein Data Bank (PDB, ID: 4KFM) as the source for the Gβ1γ2 subunit structures in this study.

Following this, the modification in free energy caused by the amino acid mutation was then analyzed using RMSD and RMSF calculations. The results are shown in the following chapter.

Run number	ΔG (Tripeptide), kJ/mol	ΔG (Gβ1γ2), kJ/mol
1	-21.82 ± 0,37	-4,29 ± 0,99
2	-20,91 ± 0,43	0,39 ± 2,06
3	-20,36 ± 0,43	1,65 ± 1,14
4	-20,16 ± 0,44	2,93 ± 0,71
5	-20,76 ± 0,41	1,09 ± 0,96

Table 1: *Free energy changes during MD simulation for tripeptide and Gβ1γ2 subunit.*

6.1 Calculation of the Free Energy Change Due to G64V in the Tripeptide

The following histograms show the non-equilibrium molecular dynamics (NEMD) simulations performed for the G64V mutation. To calculate the free energy, the BAR method was used. As seen in the snapshots, the data is divided into two parts. The left side displays the forward and backward processes of the respective initial structures where on the right side, the range of work measurement with their respective intersections, which determine the energy difference, is shown. These snapshots represent free energy calculations for the conversion from WT to G64V in the tripeptide model.

Colors in the graph: Green = Forward; Blue = Backward

Run1	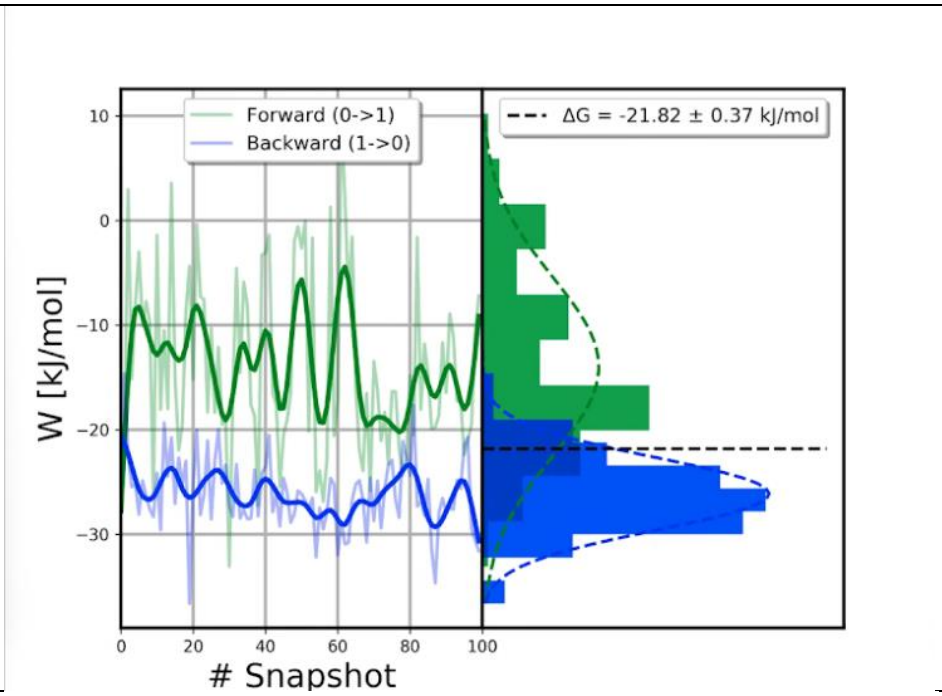
Run2	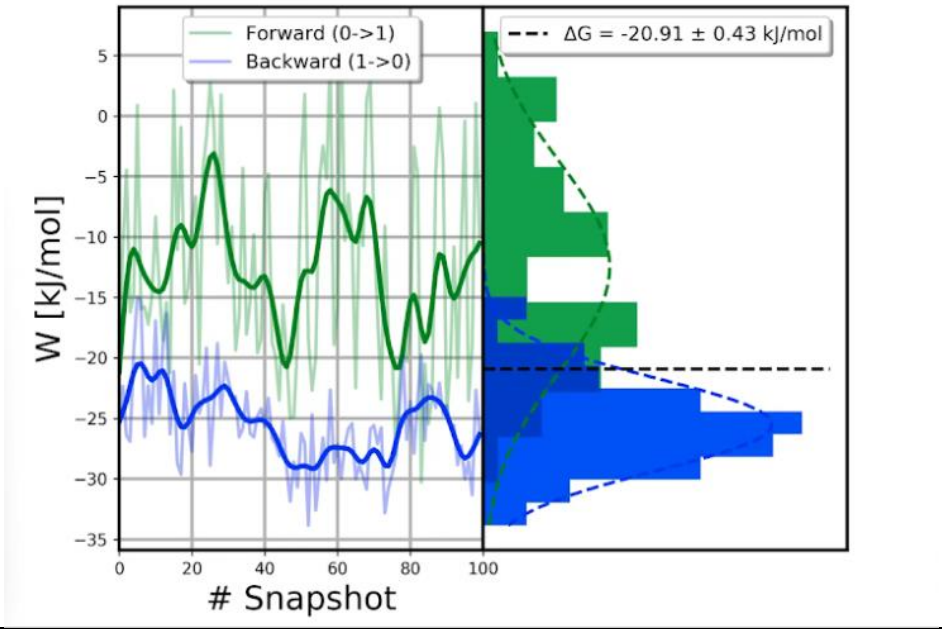

Run3	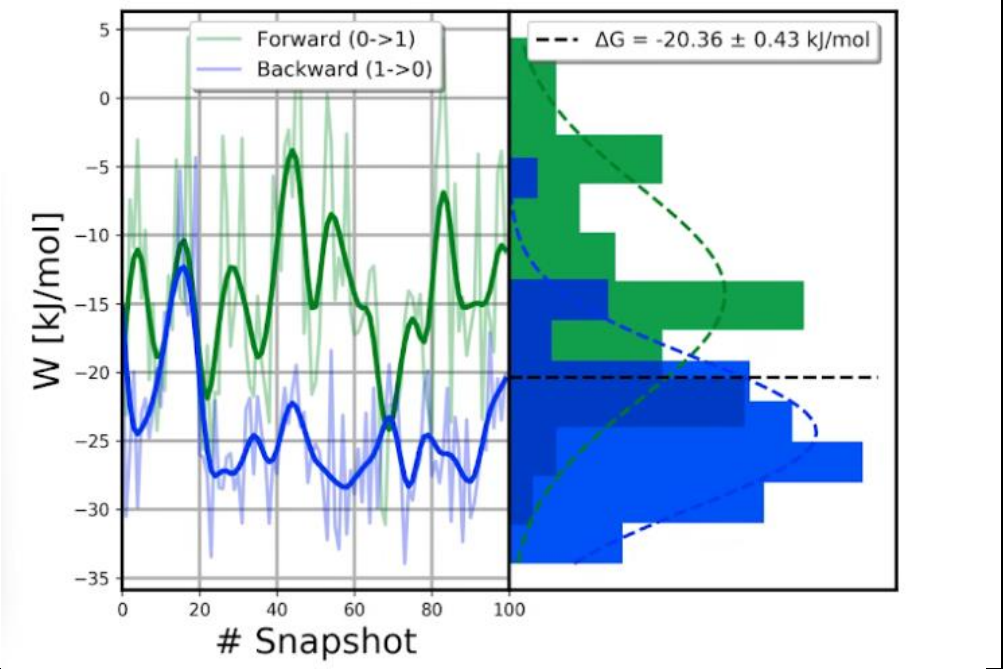 Forward (0->1) Backward (1->0) ΔG = -20.36 ± 0.43 kJ/mol W [kJ/mol] # Snapshot
Run4	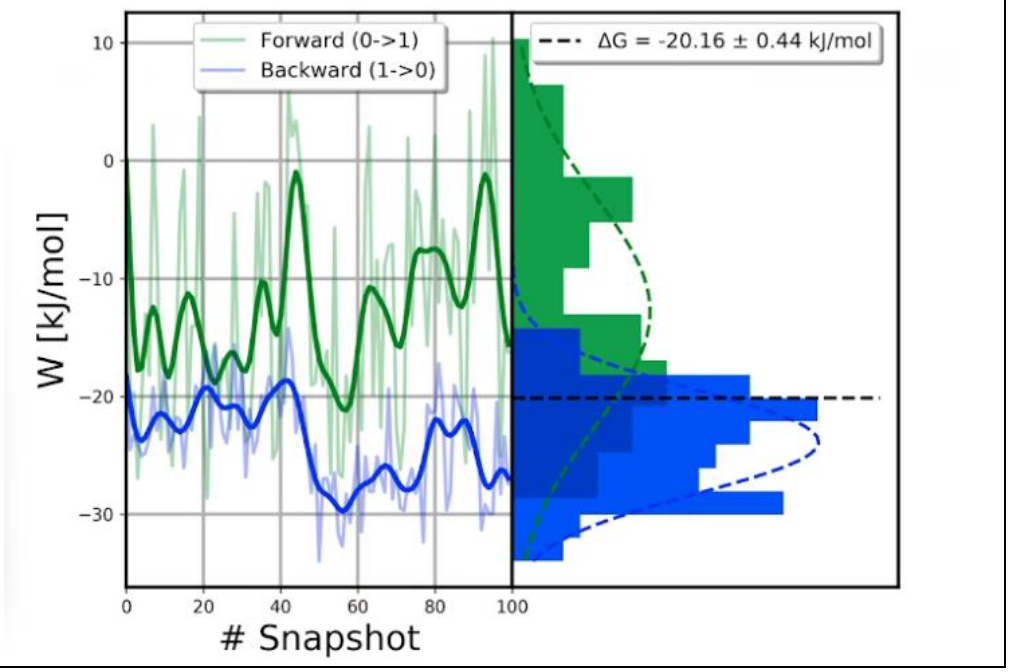 Forward (0->1) Backward (1->0) ΔG = -20.16 ± 0.44 kJ/mol W [kJ/mol] # Snapshot

Run5	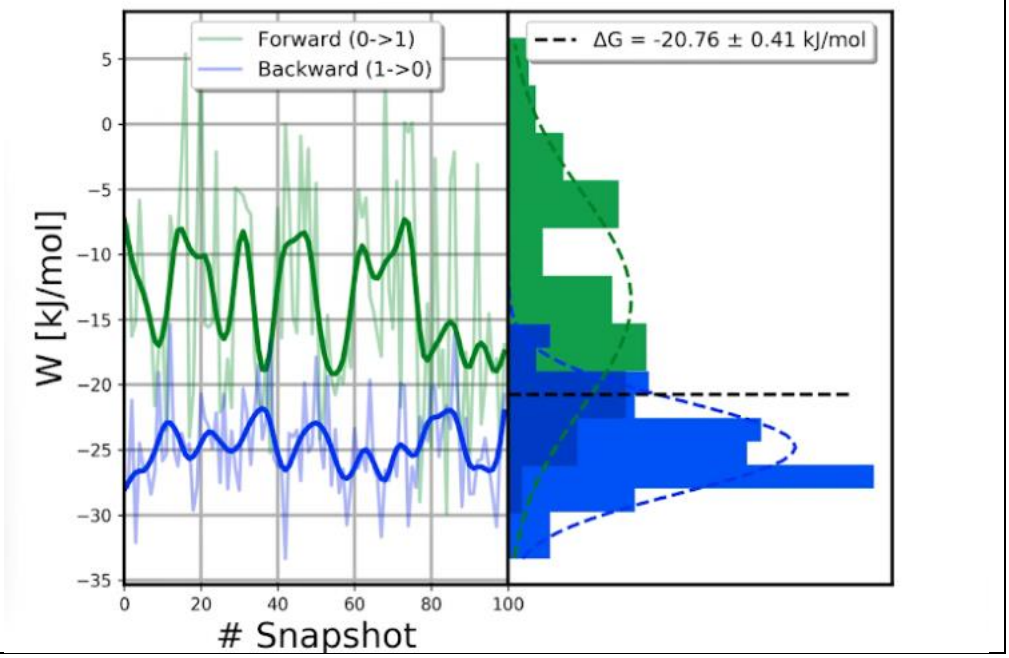

Figure 14: *Snapshots from the free energy calculation of the conversion from Wildtype to the G64V mutation in the tripeptide.*

Calculation of the energy change for the five runs for the tripeptide is as follows:

$$\Delta G_{\text{avg}}^{\text{tripep}} = \frac{-21{,}82 + (-20{,}91) + (-20{,}36) + (-20{,}16) + (-20{,}76)}{5} = -20{,}802\ \text{kJ/mol}$$

6.2 Calculation of the free energy change caused by the G64V mutation in the Gβγ subunit

The following snapshots show the 5 runs of the MD simulation and the calculation of the conversion from Wildtype to the G64V mutation in the Gβ1γ2 subunit. The snapshots on the left side of the diagram show the work done for the forward and backward transformations of the structure. On the right, the distribution of the work values with the corresponding intersections that determine the energy difference is shown. These snapshots represent the free energy calculations for the conversion from WT to G64V for the Gβ1γ2 subunit model.

Colors in the graph: Green: Forward; Blue: Backward

Run1	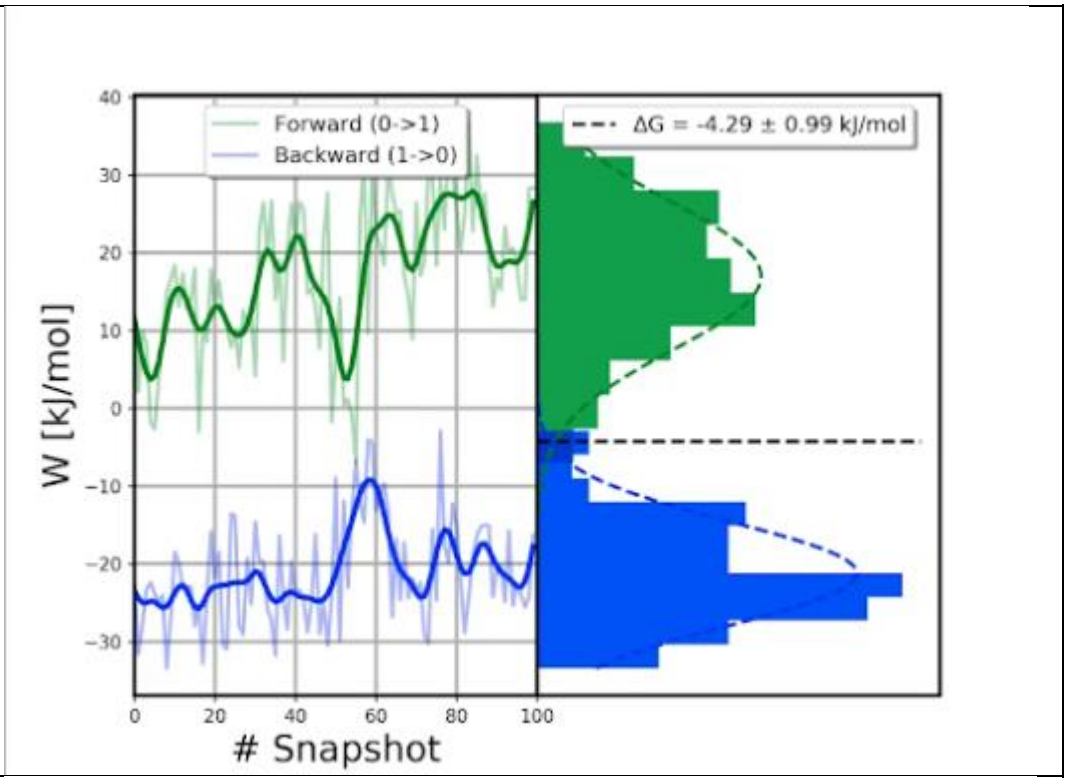
Run2	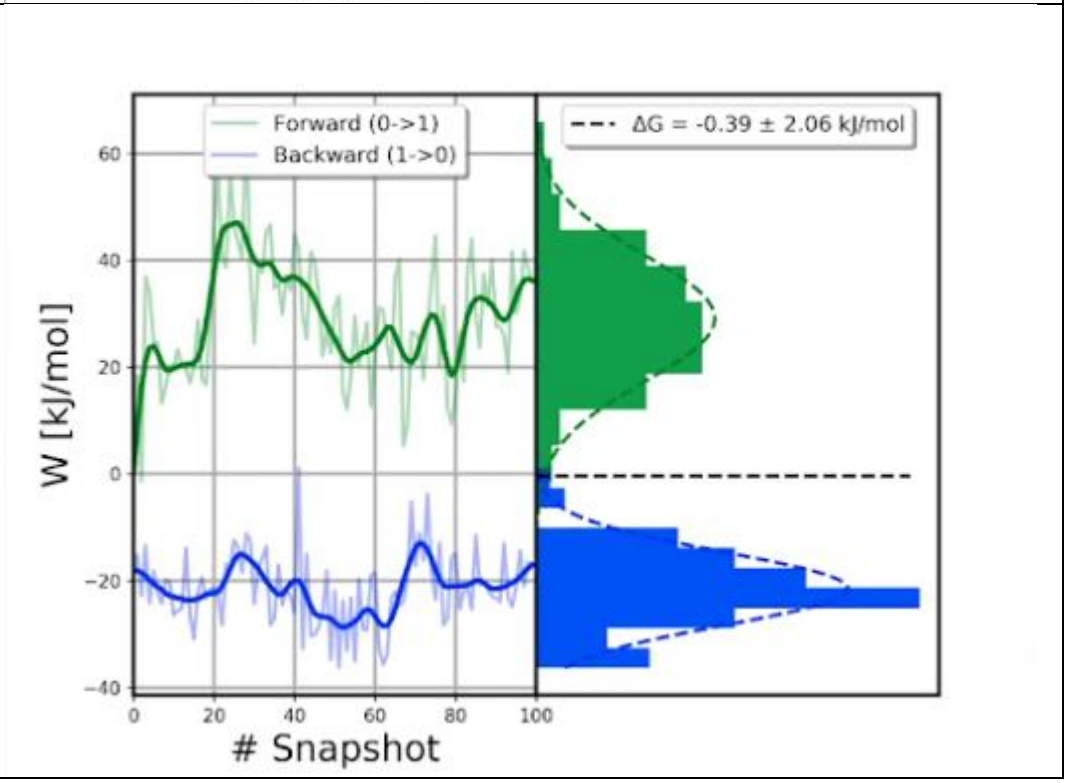

Run3	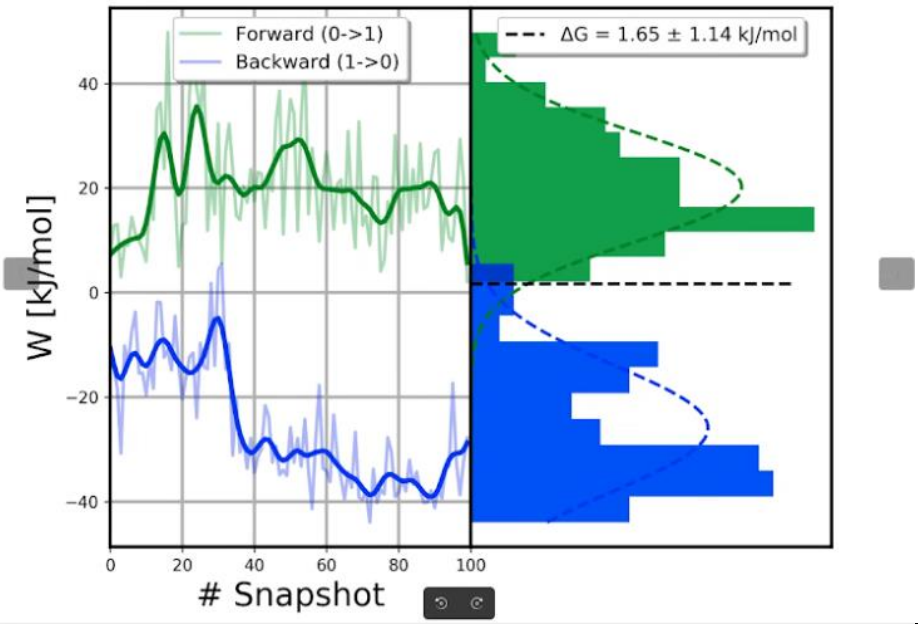 Forward (0->1) Backward (1->0) ΔG = 1.65 ± 1.14 kJ/mol W [kJ/mol] # Snapshot
Run4	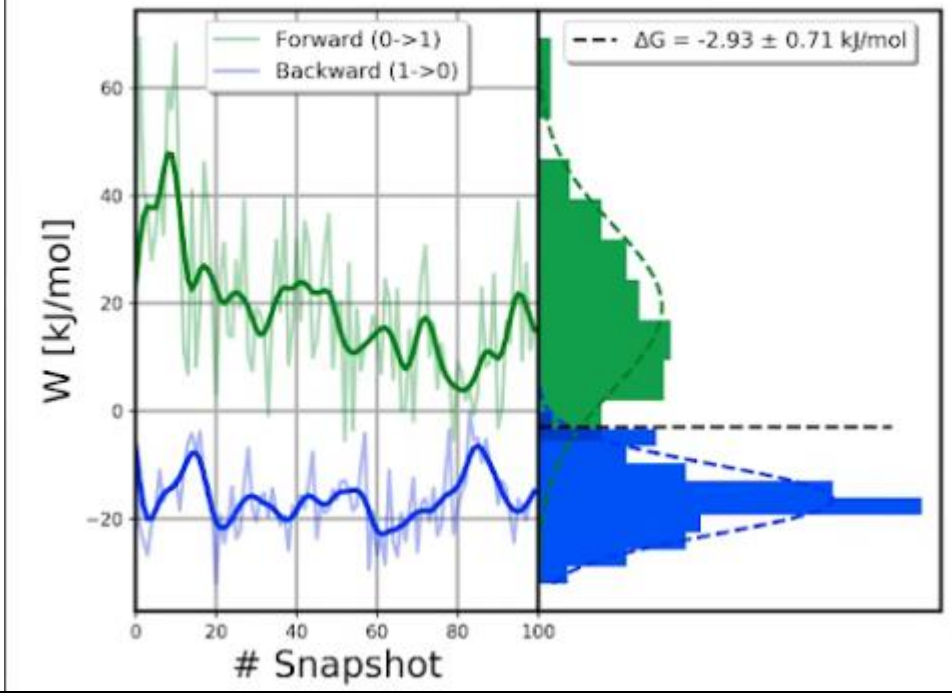 Forward (0->1) Backward (1->0) ΔG = -2.93 ± 0.71 kJ/mol W [kJ/mol] # Snapshot

Run5	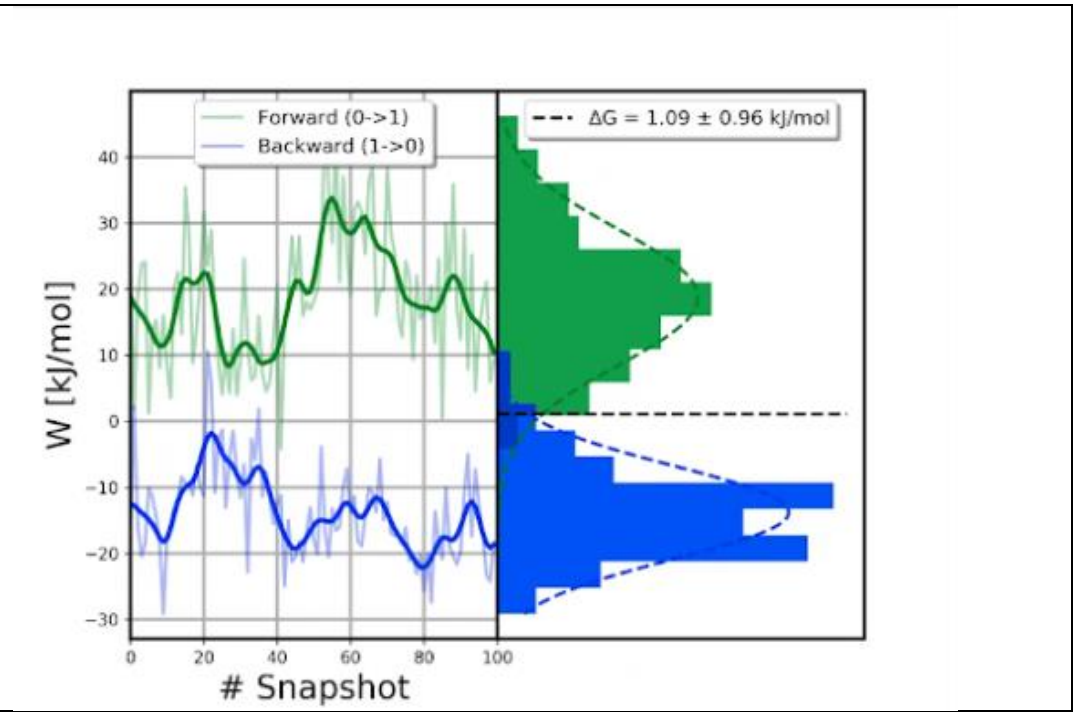

Figure 15: *Snapshots of the free energy calculation from wild type to the G64V mutation in the Gβγ subunit.*

6.3 ΔΔG Mutation Results

The following formula is used to calculate $\Delta\Delta G_{\text{Folding}}^{(\text{Mutation})}$:

$$\Delta\Delta G_{Folding}^{Mutation} = \Delta G^{\text{Protein}} - \Delta G_{tripeptide}^{apo}$$

(Aldeghi et al., 2019)

The formula shown above was used for five runs. The results are as follows:

Run number	ΔΔG, kJ/mol
1	16,52
2	21,20
3	22,46
4	17,88
5	21,90
Average	19,99

Table 2: *Overview of the Calculated ΔΔG results.*

The clearly positive result of the ΔΔG average value of 19.99 kJ/mol shows that the mutation increases the free energy and that G64V destabilizes the Gβ1γ2 complex.

6.4 Root Mean Square Deviation (RMSD)

To make the extent of the effect of the G64V mutation in the Gβ1γ2 subunit visible, RMSD was calculated. Calculations for both the wild type and the mutation were performed using MD simulations.

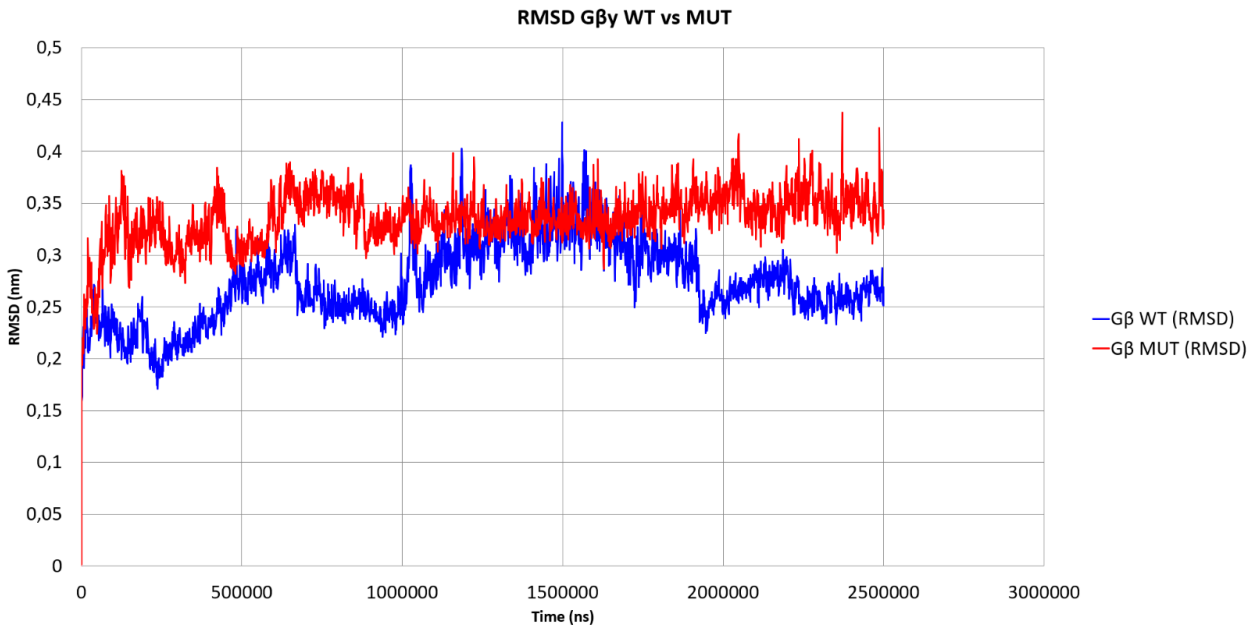

Figure 16: *RMSD calculation and graph of the Gβγ subunits for both the wild type and the G64V mutation. Blue graph: wild type; Red graph: mutation.*

The RMSD values for the wild type (Gβ1-WT) range on average between 0.20 nm and 0.35 nm and show an overall stable progression over time with minimal fluctuations. In direct comparison Figure 16 shows the Gβ-G64V mutation consistently higher, at approximately 0.30 nm to 0.42 nm, and displaying slight dynamics, indicating that the mutation leads to a minor structural destabilization.

6.5 Root Mean Square Fluctuation (RMSF)

Root Mean Square Fluctuation (RMSF) makes it possible to detect local flexibilities of specific amino acid residues, even in an overall converged system. To capture potential effects of the G64V mutation on the structural mobility of the Gβ1γ2 complex, an RMSF-based analysis was performed. For this purpose, the residue fluctuations of both variants, wild type and mutant,

were determined over the course of a 250 ns MD simulation.The results are presented comparatively in Figure 17 and illustrate the fluctuations within the Gβ1 subunit.

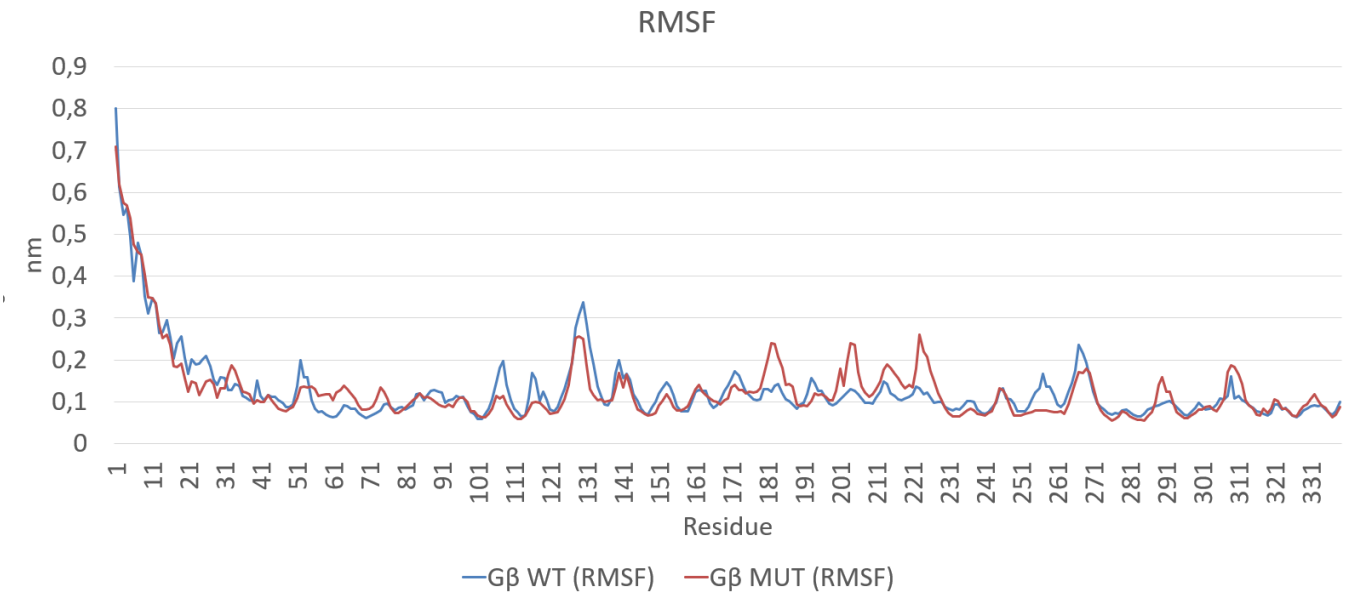

Figure 17: *RMSF calculation and graph for the Gβ1γ2 subunit over a 250 ns MD simulation timeframe for the Gβ1γ2 G model in water. (Blue: Wild type, Red: Mutation)*

The RMSF comparison between the Gβ1 wild type (WT) and the G64V mutant shows overall similar fluctuation patterns, indicating that the mutation does not cause massive structural changes in the entire complex. When looking at the specific position, it shows a distinct difference when it comes to flexibility. A particularly noticeable increase in fluctuation was observed in the region of residues approximately 220 to 230 in the mutant compared to the WT. This region might be structurally sensitive to the G64V substitution, even though it is not located directly at the mutation site. Discrete differences are also visible around residues 130 to 140.According to structural models, the affected regions are mainly situated on the surface of the Gβ1 complex, and therefore may influence intermolecular interactions, such as those with effectors or regulatory proteins. Even though the changes stay localized, they could still have functional consequences, particularly regarding protein-protein interactions.

6.6 Residue Energie Analysis

The structure of a protein is stabilized by multiple physical forces, which together determine its overall behavior. In the following, we analyze the Coulomb interactions (Figure 18) and Lennard-Jones interactions (Figure 19). Coulomb interactions are considered for electrostatic effects, such as salt bridges and hydrogen bonds, over relatively long distances. On the other hand, the Lennard-Jones interactions describe a quite short-range van der Waals forces and are important for the structural packing of residues and hydrophobic contacts. Residue interaction (Figure 21) analysis evaluates nonbonded interactions between specific amino acids, revealing local destabilization or modification in packing due to the mutation. Water interaction analysis (Figure 20) provides insight into solvation effects and dynamic stability, for example, highlighting regions of transient instability or even increased fluctuations. Considering all this analysis gives knowledge to a realistic representation of the protein structure. They allow insights into the origins of stability changes caused by mutations. Coulomb interaction: Figure 18 shows significant changes at key contact residues Ser67 and Asp66. Overall, the alterations at Asp66 and Ser67 indicate a local loss of electrostatic interactions caused by the G64V mutation. The G64V mutation results in a local loss of interactions at residues of Ser67 and Asp66, while more distal regions remain largely unaffected.

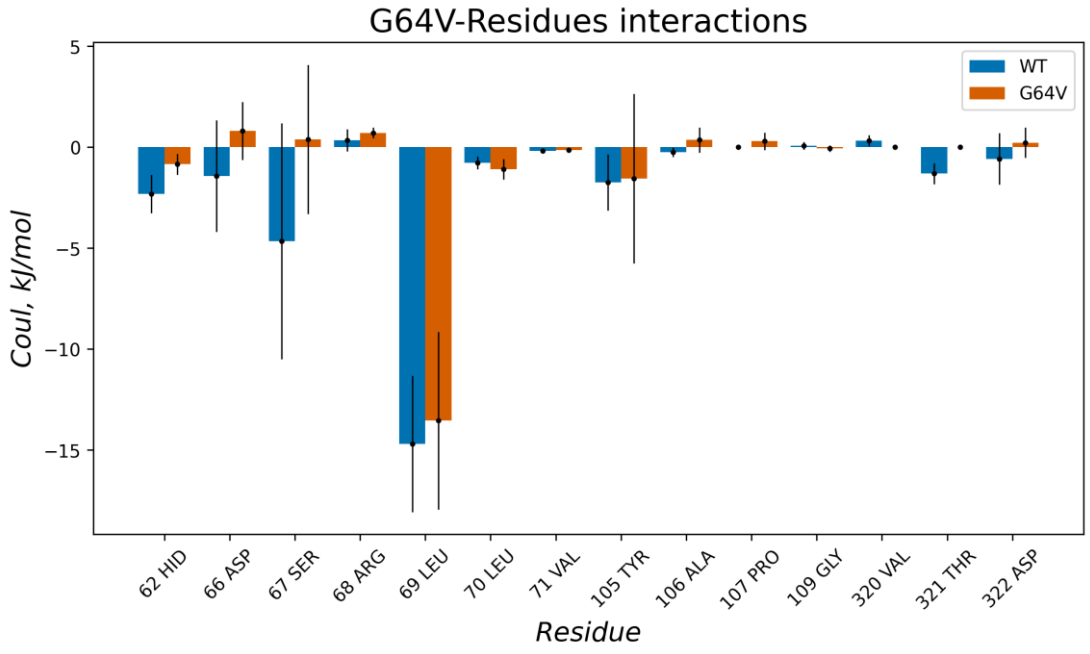

Figure 18: *Residue-wise comparison of nonbonded interaction energies between wild type and G64V mutant, highlighting local effects at key residue*

Lennard Jones interaction: In Figure 19 the Lennard-Jones energy analysis shows in general negative values, indicating van der Waals interactions. The largest differences are observed at residues of Hid62 and Tyr105, with Asp66 showing only a very small change. For the remaining residues, where differences appear minimal, indicating that the mutation primarily has a local effect and does not impact global van der Waals interactions.

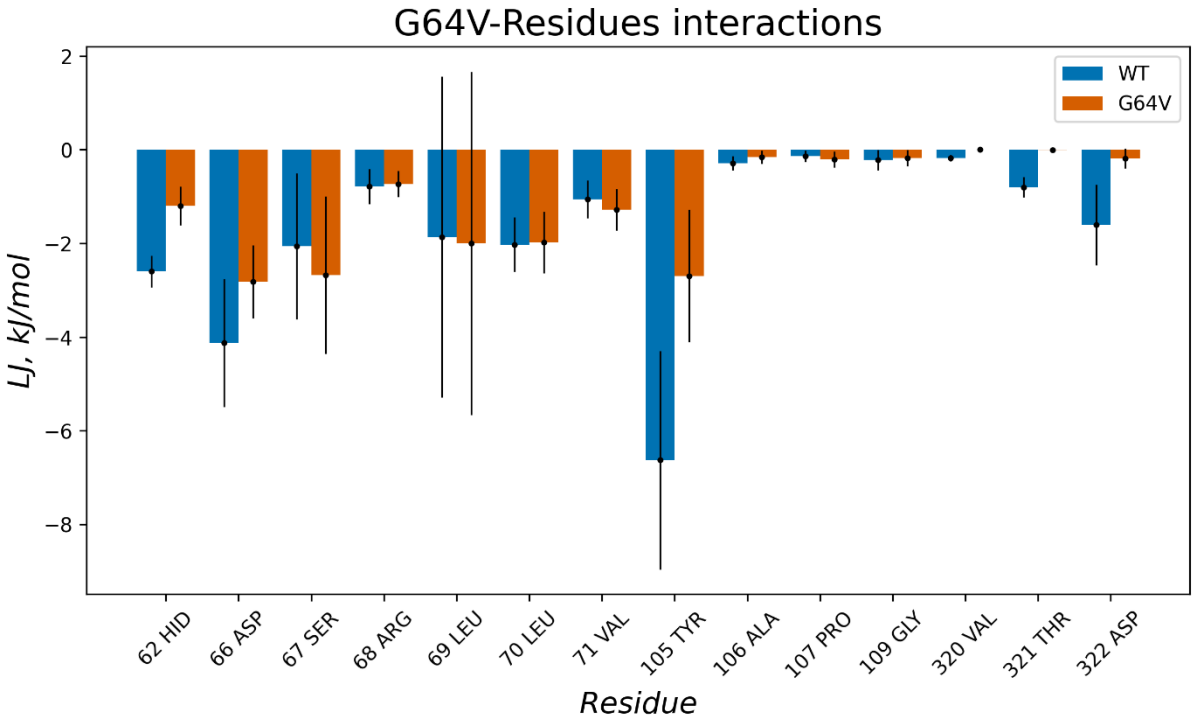

Figure 19: *Residue-wise Lennard-Jones interaction energies for wild type and G64V mutant, showing overall favorable interactions with only local differences at selected residues.*

Water Interaction: In Figure 20, the graph describes how stable the protein is over time with regard to its interaction with water, which serves as a measure of solvation and dynamic stability. The x-axis represents time, while the y-axis shows the nonbonded interaction with water. As observed, the wild type values are negative with a moderate fluctuation. Indicating that water interactions remain stable throughout the simulation. The G64V mutation does not change the residue's interactions with water.

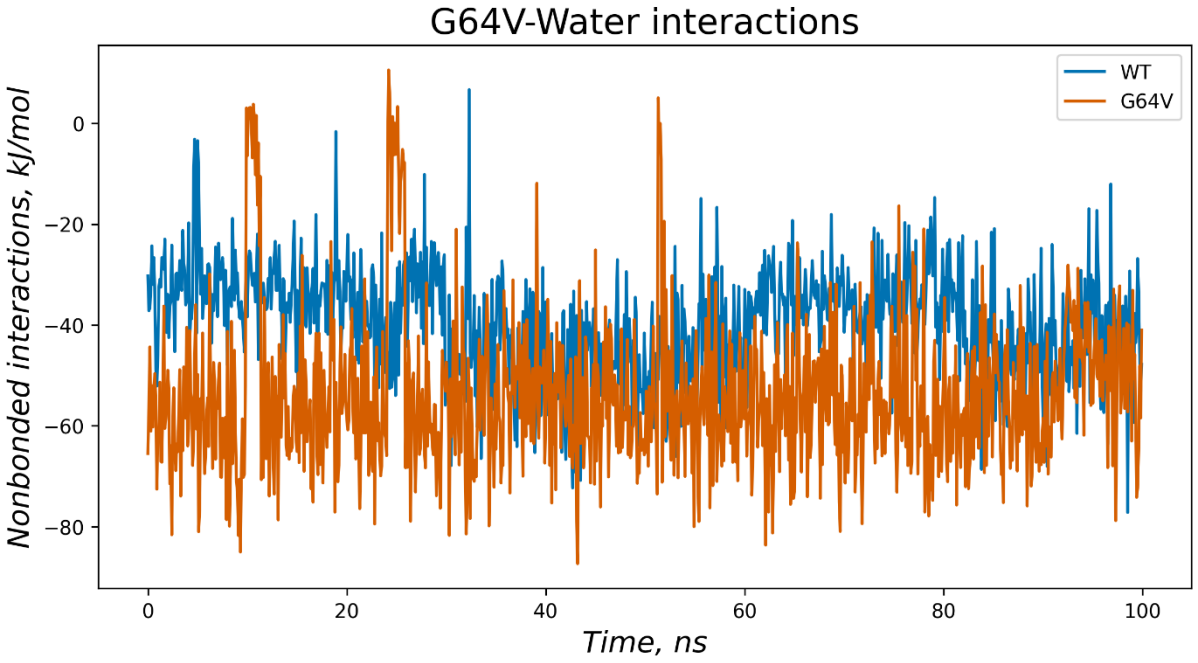

Figure 20: *Protein–water nonbonded interactions over time for wild type and G64V mutant, showing stable solvation in the wild type and increased fluctuations in the mutant.*

Residue Interaction: In Figure 21, the residue interaction analysis is shown. The x-axis here represents the individual residues interacting in the wild type and mutant. The y-axis shows the average nonbond interactions. The largest differences between wild type and mutant are observed for residues 62His, 66Asp, 67Ser, and 105Tyr. In conclusion, the residue analysis shows that the G64V mutation locally destabilizes a number of residues.

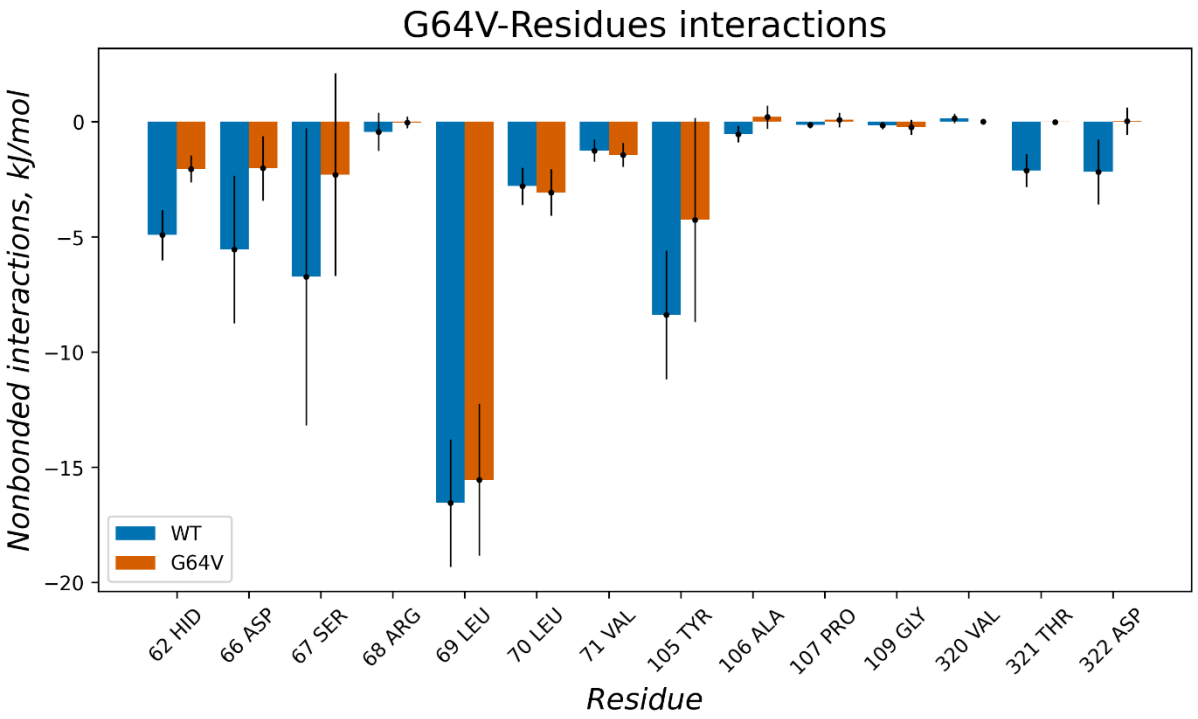

Figure 21: *Residue-wise averaged nonbonded interaction energies for wild type and G64V mutant, highlighting local weakening of interactions near the mutation site and corresponding transient effects observed in the water interaction analysis.*

7. Discussion

The GNB1 encephalopathy, caused by point mutations such as G64V in the Gβ1γ2 subunit, was investigated in the study by Lohmann et al. (2017). Their work provided insights into both the dynamics and stability of the dimer, which were influenced to varying degrees by these mutations. The free energy differences (ΔG) between the wild type and the G64V mutation were calculated, for tripeptide and Gβ1γ2 complex, followed by the determination of the energy differences caused specifically by the point mutation (ΔΔG). It was found that the G64V point mutation, with an average ΔΔG value of 19.99 kJ/mol, indicates that the mutation increases the free energy suggesting a destabilization of the Gβ1γ2 complex. The RMSD values of the mutation graph, compared to those of the wild type, show clear fluctuations between 0.30 nm and 0.42 nm, suggesting a change in Gβ1 structure. The RMSF values of the mutation also show a number of differences compared to the wild type. In the region around residues 126 - 140, there are small changes likely affecting cysteine, leucine, and glycine residues. In the range of 170-175, differences are identified involving glycine and asparagine. Also a high fluctuation in the region of residues 220 -230 are noted, affecting serine and leucine. These residues are in the outer region of the WD40 domains of the Gβ subunit and could allow more access to interaction partners because of the mutation. The result is consistent with the BRET analyses in the Lohmann study (2017), which showed that a weaker BRET signal for the G64V mutation is explained by a low expression of the Gβ1γ2 (Lohmann et al., 2017). More insides into the effects of G64V were provided and evaluated through additional analyses of local interactions. The mutation locally weakens van der Waals (Lennard-Jones) and nonbonded (Coulomb) interactions at key residues, including His62, Asp66, Ser67 and Tyr105. The MD simulations show only small structural changes in the Gβ1γ2complex carrying the G64V mutation, suggestion that the mutation has a great effect on the Gβ1 expression that on the structural stability in general (Lohmann et al., 2017).

8. Conclusion

Overall, it can be stated that the G64V mutation induces a moderate destabilization of the Gβγ dimer, consistent with RMSD analysis showing that the global structure remains largely stable. The local flexibility analyses (RMSF) show small changes in surface regions but no major structural changes. Reduced BRET signals have been reported for the G64V mutation and are likely related to reduced Gβ1 expression. Our results align with the study by Lohmann et al. (2017). In conclusion, these results highlight that G64V mutation can have an effect of protein function through mechanisms such as changes at specific interaction sites. Future studies combining biophysical experiments, structural analysis, and targeted molecular screening would be valuable. The studies could give clarity on the molecular basis of the effects and their contribution to GNB1 encephalopathy.

9. References

Abraham, M. J., Murtola, T., Schulz, R., Páll, S., Smith, J. C., Hess, B., & Lindahl, E. (2015). GROMACS: High performance molecular simulations through multi-level parallelism from laptops to supercomputers. *SoftwareX*, *1–2*, 19–25. https://doi.org/10.1016/j.softx.2015.06.001

Aldeghi, M., De Groot, B. L., & Gapsys, V. (2019). Accurate Calculation of Free Energy Changes upon Amino Acid Mutation. In T. Sikosek (Hrsg.), *Computational Methods in Protein Evolution* (Bd. 1851, S. 19–47). Springer New York. https://doi.org/10.1007/978-1-4939-8736-8_2

Andrade, X., Castro, A., Zueco, D., Alonso, J. L., Echenique, P., Falceto, F., & Rubio, A. (2009). A modified Ehrenfest formalism for efficient large-scale ab initio molecular dynamics. *Journal of Chemical Theory and Computation*, *5*(4), 728–742. https://doi.org/10.1021/ct800518j

Atkins, P., De Paula, J., & Keeler, J. (2017). *Atkins' physical chemistry (11th ed.)* (11. Aufl.). Oxford University Press.

Breimann, S., Kamp, F., Steiner, H., & Frishman, D. (2024). AAontology: An Ontology of Amino Acid Scales for Interpretable Machine Learning. *Journal of Molecular Biology*, *436*(19), 168717. https://doi.org/10.1016/j.jmb.2024.168717

Case, D. A., Cheatham, T. E., Darden, T., Gohlke, H., Luo, R., Merz, K. M., Onufriev, A., Simmerling, C., Wang, B., & Woods, R. J. (2005). The Amber biomolecular simulation programs. *Journal of Computational Chemistry*, *26*(16), 1668–1688. https://doi.org/10.1002/jcc.20290

Chung, Y. K., & Wong, Y. H. (2021). Re-examining the 'Dissociation Model' of G protein activation from the perspective of Gβγ signaling. *The FEBS Journal*, *288*(8), 2490–2501. https://doi.org/10.1111/febs.15605

Colombo, S., Reddy, H. P., Petri, S., Williams, D. J., Shalomov, B., Dhindsa, R. S., Gelfman, S., Krizay, D., Bera, A. K., Yang, M., Peng, Y., Makinson, C. D., Boland, M. J., Frankel, W. N., Goldstein, D. B., & Dascal, N. (2023). Epilepsy in a mouse model of GNB1 encephalopathy arises from altered potassium (GIRK) channel signaling and is alleviated by a GIRK inhibitor. *Frontiers in Cellular Neuroscience*, *17*, 1175895. https://doi.org/10.3389/fncel.2023.1175895

Da Silva, J. D., Costa, M. D., Almeida, B., Lopes, F., Maciel, P., & Teixeira-Castro, A. (2021). Case Report: A Novel GNB1 Mutation Causes Global Developmental Delay With Intellectual Disability and Behavioral Disorders. *Frontiers in Neurology*, *12*, 735549. https://doi.org/10.3389/fneur.2021.735549

De Vivo, M., Masetti, M., Bottegoni, G., & Cavalli, A. (2016). Role of Molecular Dynamics and Related Methods in Drug Discovery. *Journal of Medicinal Chemistry*, *59*(9), 4035–4061. https://doi.org/10.1021/acs.jmedchem.5b01684

El Khamlichi, C., Reverchon-Assadi, F., Hervouet-Coste, N., Blot, L., Reiter, E., & Morisset-Lopez, S. (2019). Bioluminescence Resonance Energy Transfer as a Method to Study Protein-Protein Interactions: Application to G Protein Coupled Receptor Biology. *Molecules*, *24*(3), 537. https://doi.org/10.3390/molecules24030537

Hassan, B. A., Milicaj, J., Ramirez-Mondragon, C. A., Sham, Y. Y., & Taylor, E. A. (2022). Ligand-Induced Conformational and Dynamical Changes in a GT-B Glycosyltransferase: Molecular Dynamics Simulations of Heptosyltransferase I Complexes. *Journal of Chemical Information and Modeling*, *62*(2), 324–339. https://doi.org/10.1021/acs.jcim.1c00868

Joshi, R., Tripathi, M., Gupta, P., & Gupta, Y. K. (2014). Effect of clobazam as add-on antiepileptic drug in patients with epilepsy. *The Indian Journal of Medical Research*, *140*(2), 209–215.

Kameda, T., Awazu, A., & Togashi, Y. (2022). Molecular dynamics analysis of biomolecular

systems including nucleic acids. *Biophysics and Physicobiology*, *19*(0), n/a. https://doi.org/10.2142/biophysico.bppb-v19.0027

Kerppola, T. K. (2008). Bimolecular Fluorescence Complementation: Visualization of Molecular Interactions in Living Cells. In *Methods in Cell Biology* (Bd. 85, S. 431–470). Elsevier. https://doi.org/10.1016/S0091-679X(08)85019-4

Lohmann, K., Masuho, I., Patil, D. N., Baumann, H., Hebert, E., Steinrücke, S., Trujillano, D., Skamangas, N. K., Dobricic, V., Hüning, I., Gillessen-Kaesbach, G., Westenberger, A., Savic-Pavicevic, D., Münchau, A., Oprea, G., Klein, C., Rolfs, A., & Martemyanov, K. A. (2017). Novel *GNB1* mutations disrupt assembly and function of G protein heterotrimers and cause global developmental delay in humans. *Human Molecular Genetics*, ddx018. https://doi.org/10.1093/hmg/ddx018

Malerba, N., De Nittis, P., & Merla, G. (2019). The Emerging Role of Gβ Subunits in Human Genetic Diseases. *Cells*, *8*(12), 1567. https://doi.org/10.3390/cells8121567

Meriney, S. D., & Fanselow, E. E. (2019). Metabotropic G-Protein-Coupled Receptors and Their Cytoplasmic Signaling Pathways. In *Synaptic Transmission* (S. 245–273). Elsevier. https://doi.org/10.1016/B978-0-12-815320-8.00012-0

Nasvytis, M., Čiauškaitė, J., & Jurkevičienė, G. (2024). GNB1 Encephalopathy: Clinical Case Report and Literature Review. *Medicina*, *60*(4), 589. https://doi.org/10.3390/medicina60040589

Ohashi, K., Kiuchi, T., Shoji, K., Sampei, K., & Mizuno, K. (2012). Visualization of Cofilin-actin and Ras-Raf Interactions by Bimolecular Fluorescence Complementation Assays Using a New Pair of Split Venus Fragments. *BioTechniques*, *52*(1), 45–50. https://doi.org/10.2144/000113777

Ojanperä, A., Havu, V., Lehtovaara, L., & Puska, M. (2012). Nonadiabatic Ehrenfest molecular dynamics within the projector augmented-wave method. *The Journal of Chemical Physics*, *136*(14), 144103. https://doi.org/10.1063/1.3700800

Petrovski, S., Küry, S., Myers, C. T., Anyane-Yeboa, K., Cogné, B., Bialer, M., Xia, F., Hemati, P., Riviello, J., Mehaffey, M., Besnard, T., Becraft, E., Wadley, A., Politi, A. R., Colombo, S., Zhu, X., Ren, Z., Andrews, I., Dudding-Byth, T., … Goldstein, D. B. (2016). Germline De Novo Mutations in GNB1 Cause Severe Neurodevelopmental Disability, Hypotonia, and Seizures. *American Journal of Human Genetics*, *98*(5), 1001–1010. https://doi.org/10.1016/j.ajhg.2016.03.011

Reddy, H. P., Yakubovich, D., Keren-Raifman, T., Tabak, G., Tsemakhovich, V. A., Pedersen, M. H., Shalomov, B., Colombo, S., Goldstein, D. B., Javitch, J. A., Bera, A. K., & Dascal, N. (2021). Encephalopathy-causing mutations in Gβ1 (GNB1) alter regulation of neuronal GIRK channels. *iScience*, *24*(9), 103018. https://doi.org/10.1016/j.isci.2021.103018

Reinhardt, M., & Grubmüller, H. (2021). Small-sample limit of the Bennett acceptance ratio method and the variationally derived intermediates. *Physical Review E*, *104*(5), 054133. https://doi.org/10.1103/PhysRevE.104.054133

Revah-Politi, A., Sands, T. T., Colombo, S., Goldstein, D. B., & Anyane-Yeboa, K. (2020). *GNB1 Encephalopathy* (S. 1–9). https://www.ncbi.nlm.nih.gov/books/NBK554743/

Ribaldone, C., & Casassa, S. (2024). Born–Oppenheimer Molecular Dynamics with a Linear Combination of Atomic Orbitals and Hybrid Functionals for Condensed Matter Simulations Made Possible. Theory and Performance for the Microcanonical and Canonical Ensembles. *Journal of Chemical Theory and Computation*, *20*(9), 3954–3975. https://doi.org/10.1021/acs.jctc.3c01231

Salahpour, A. (2012). BRET biosensors to study GPCR biology, pharmacology, and signal transduction. *Frontiers in Endocrinology*, *3*. https://doi.org/10.3389/fendo.2012.00105

Smrcka, A. V., & Fisher, I. (2019). G-protein βγ subunits as multi-functional scaffolds and transducers in G-protein-coupled receptor signaling. *Cellular and Molecular Life Sciences: CMLS*, *76*(22), 4447–4459. https://doi.org/10.1007/s00018-019-03275-2

Stefl, S., Nishi, H., Petukh, M., Panchenko, A. R., & Alexov, E. (2013). Molecular Mechanisms of Disease-Causing Missense Mutations. *Journal of Molecular Biology*, *425*(21), 3919–3936. https://doi.org/10.1016/j.jmb.2013.07.014

Torrens-Fontanals, M., Stepniewski, T. M., Aranda-García, D., Morales-Pastor, A., Medel-Lacruz, B., & Selent, J. (2020). How Do Molecular Dynamics Data Complement Static Structural Data of GPCRs. *International Journal of Molecular Sciences*, *21*(16), 5933. https://doi.org/10.3390/ijms21165933

Vickers, T. A., & Crooke, S. T. (2016). Development of a Quantitative BRET Affinity Assay for Nucleic Acid-Protein Interactions. *PLOS ONE*, *11*(8), e0161930. https://doi.org/10.1371/journal.pone.0161930

Wall, M. A., Coleman, D. E., Lee, E., Iñiguez-Lluhi, J. A., Posner, B. A., Gilman, A. G., & Sprang, S. R. (1995). The structure of the G protein heterotrimer Giα1β1γ2. *Cell*, *83*(6), 1047–1058. https://doi.org/10.1016/0092-8674(95)90220-1

Xu, X., Liu, A., Liu, S., Ma, Y., Zhang, X., Zhang, M., Zhao, J., Sun, S., & Sun, X. (2023). Application of molecular dynamics simulation in self-assembled cancer nanomedicine. *Biomaterials Research*, *27*(1), 39. https://doi.org/10.1186/s40824-023-00386-7

Zou, Y., Ewalt, J., & Ng, H.-L. (2019). Recent Insights from Molecular Dynamics Simulations for G Protein-Coupled Receptor Drug Discovery. *International Journal of Molecular Sciences*, *20*(17), 4237. https://doi.org/10.3390/ijms20174237

10. Internet references

www1: GNB1 Foundation, Retrieved March, 2026; https://www.gnb1.org/

www2: MolView., Retrieved July, 2025; https://app.molview.com/